Forebrain excitatory neuron-specific loss of Brpf1 attenuates excitatory synaptic transmission and impairs spatial and fear memory

Baicheng Zhao[1, #], Hang Zhang[1, #], Ying Liu[1, #], Gaoyu Zu[1], Yuxiao Zhang[2, 3, 4], Jiayi Hu[1], Shuai Liu[2, 3, 4], Linya You[1, 5, *]

https://doi.org/10.4103/1673-5374.385307

Date of submission: February 6, 2023

Date of decision: June 10, 2023

Date of acceptance: July 19, 2023

Date of web publication: September 22, 2023

From the Contents

Introduction	1133
Methods	1134
Results	1135
Discussion	1138

Graphical Abstract

Brpf1 loss in CAMKIIa-Cre expressing cells led to reduced excitatory synaptic transmission and disrupted spatial and fear memory

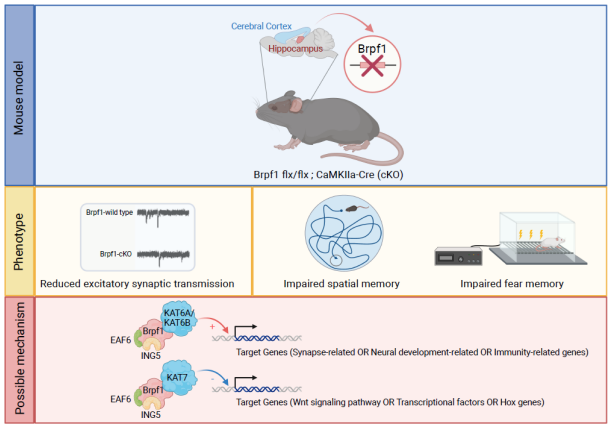

Abstract

Bromodomain and plant homeodomain (PHD) finger containing protein 1 (Brpf1) is an activator and scaffold protein of a multiunit complex that includes other components involving lysine acetyltransferase (KAT) 6A/6B/7. Brpf1, KAT6A, and KAT6B mutations were identified as the causal genes of neurodevelopmental disorders leading to intellectual disability. Our previous work revealed strong and specific expression of *Brpf1* in both the postnatal and adult forebrain, especially the hippocampus, which has essential roles in learning and memory. Here, we hypothesized that *Brpf1* plays critical roles in the function of forebrain excitatory neurons, and that its deficiency leads to learning and memory deficits. To test this, we knocked out *Brpf1* in forebrain excitatory neurons using *CaMKIIa-Cre*. We found that Brpf1 deficiency reduced the frequency of miniature excitatory postsynaptic currents and downregulated the expression of genes *Pcdhgb1*, *Slc16a7*, *Robo3*, and *Rho*, which are related to neural development, synapse function, and memory, thereby damaging spatial and fear memory in mice. These findings help explain the mechanisms of intellectual impairment in patients with BRPF1 mutation.

Key Words: behavioral test; *Brpf1*; CAMKIIa-Cre; intellectual disability; miniature excitatory postsynaptic current; mRNA-Seq

Introduction

The bromodomain and plant homeodomain (PHD) finger-containing protein 1 (BRPF1) is a scaffold protein and an activator of a tetrameric complex comprising monocytic leukemia zinc finger protein (MOZ or lysine acetylatransferase 6A (KAT6A)), MOZ-related factor (MORF or KAT6B), or histone acetyltransferase (HAT) bound to origin recognition complex subunit 1 (ORC1) (HBO1 or KAT7) and two small non-catalytic proteins, inhibitor of growth 5 (ING5) or ING4 and MYST/Esa1-associated factor 6 (MEAF6) (Ullah et al., 2008). Three of the subunits, BRPF1, KAT6A, and KAT6B, have been identified as causal genes in germline mutations associated with neurodevelopmental disorders leading to intellectual disability (Zu et al., 2022). To date, 43 individuals with a total of 30 BRPF1 mutations/variants have been reported to have a disease known as intellectual developmental disorder with dysmorphic facies and ptosis (IDDDFP) (Xu et al., 2011; Mattioli et al., 2017; Yan et al., 2017, 2020; Pode-Shakked et al., 2019; Zhao et al., 2019; Keywan et al., 2020; Naseer et al., 2020; Souza et al., 2022), and 89 patients with 75 KAT6A variants have been found to have neurodevelopmental disorders with a 100% penetrance of intellectual disability (Efthymiou et al., 2018; Trinh et al., 2018; Alkhateeb and Alazaizeh, 2019; Kennedy et al., 2019; Lin et al., 2020; Urreizti et al., 2020; Bae et al., 2021; Jiang et al., 2021; Marji et al., 2021; Korakavi et al., 2022). Additionally, more than 60 variants of KAT6B have been reported in patients with Say-Barber-Biesecker-Young-Simpson syndrome (SBBYSS or Ohdo syndrome) and genitopatellar syndrome (Brea-Fernández et al., 2019), both of which are also characterized by intellectual disability.

Our previous studies indicated that the global deletion of murine *Brpf1* is embryonically lethal at E9.5 (You et al., 2014, 2015b), and that forebrain-specific *Brpf1* loss led to early postnatal lethality and neocortical deficits, as well as hippocampal and callosal hypoplasia (You et al., 2015a, c). Following our work using mouse models, we further demonstrated that acute *Brpf1* knockdown led to attenuated excitatory and inhibitory synaptic transmission, as revealed by a decrease in miniature excitatory postsynaptic current (mEPSC) frequency in primary cultured hippocampal neurons and a reduction in miniature inhibitory postsynaptic current amplitude in medial ganglionic eminence-derived GABAergic neurons, respectively (Cao et al., 2021; Xian et al., 2021). Moreover, acute knockdown of *Brpf1* in the mouse hippocampus via viral stereo-injection tended to reduce spatial memory (Xian et al., 2021). Our expression atlas of *Brpf1* has revealed specific and strong expression of *Brpf1* in the postnatal and adult hippocampus and cortex (You et al., 2014). Relatedly, another team reported a positive correlation between BRPF1 expression and human hippocampal volume (Zhao et al., 2019).

[1]Department of Human Anatomy & Histoembryology, School of Basic Medical Sciences, Fudan University, Shanghai, China; [2]Shanghai Key Laboratory of Brain Functional Genomics (Ministry of Education), Affiliated Mental Health Center (ECNU), School of Psychology and Cognitive Science, East China Normal University, Shanghai, China; [3]Shanghai Changning Mental Health Center, Shanghai, China; [4]NYU-ECNU Institute of Brain and Cognitive Science at NYU Shanghai, Shanghai, China; [5]Key Laboratory of Medical Imaging Computing and Computer Assisted Intervention of Shanghai, Shanghai, China

*Correspondence to: Linya You, PhD, lyyou@fudan.edu.cn.

https://orcid.org/0000-0002-2569-0269 (Linya You)

#These authors contributed equally to this work.

Funding: *This study was supported by the National Natural Science Foundation of China, No. 81771228 and Shanghai Association of Science and Technology, Nos. 22WZ2501700 and 23WZ2504500 (all to LY).*

How to cite this article: *Zhao B, Zhang H, Liu Y, Zu G, Zhang Y, Hu J, Liu S, You L (2024) Forebrain excitatory neuron-specific loss of Brpf1 attenuates excitatory synaptic transmission and impairs spatial and fear memory. Neural Regen Res 19(5):1133-1141.*

In this study, we hypothesized that *Brpf1* plays critical roles in the function of postnatal forebrain excitatory neurons, and that its deficiency leads to learning and memory deficits that eventually contribute to intellectual disability. To test this hypothesis, we conditionally deleted *Brpf1* in forebrain excitatory neurons postnatally using calcium/calmodulin-dependent protein kinase II alpha (*CaMKIIa*)-*Cre* (Mayford et al., 1996). We conducted mEPSC measurements using acute brain slices, behavioral tests including open field, Morris water maze (MWM), fear conditioning, novel object recognition, three-chamber test, and repetitive self-grooming, and RNA sequencing (RNA-Seq) to understand the electrophysiological, behavioral, and molecular impacts of *Brpf1* deletion on forebrain excitatory neurons, respectively.

Methods

Animals

All animal experiments were approved by the Animal Care and Use Committee of Fudan University (Shanghai, China) on February 23, 2017 (approval No. 20170223-121). All mice were produced in the Fudan University animal facility by intercrossing heterozygous knockout male and female mice ($Brpf1^{flx/+}$ mice without cre). The mice had *ad libitum* access to food and were housed in a facility with a 12-hour light/dark cycle at 18–23°C and 40–60% humidity. The wild type (WT) group comprised $Brpf1^{flx/flx}$ mice without cre and $Brpf1^{flx/+}$ mice without cre, and the conditional knockout (cKO) group included $Brpf1^{flx/flx}$ mice with cre. We used adult male C57BL/6J mice from the WT and cKO groups (both at 2 and 6 months of age, respectively, with a body weight of about 25–35 g, from Saiye Biotechnology (Suzhou), license No. SCXK (Su) 2022-0016) for histological examinations, electrophysiological measurements, RNA-Seq, reverse transcription quantitative polymerase chain reaction (RT-qPCR), and behavioral tests. Most of the experiments were performed on 2-month-old mice. The mice were not distributed randomly but assigned to the 2 groups, WT and cKO, according to genotype. The experimenters were blind to the genotype information/grouping when conducting the experiments.

Generation of Brpf1 conditional knockout mice and genotyping

To generate mice with cell-type specific deletion of *Brpf1*, we crossed $Brpf1^{flx/flx}$ mice (Saiye, Suzhou, China) with mice expressing Cre recombinase under the CAMKIIa promoter, driving *Cre* expression in the forebrain and especially CA1 pyramidal cells in the hippocampus starting in the 3rd–4th week after birth (B6.Cg-Tg(Camk2a-cre)T29-1Stl/J, Jackson Laboratory, Bar Harbor, ME, USA, stock# 005359, RRID: IMSR_JAX:005359). The $Brpf1^{flx/+}$; *CaMKIIa-Cre*$^{+}$ heterozygous progeny were subsequently intercrossed to generate the $Brpf1^{flx/flx}$; *CaMKIIa-Cre* (cKO) strain. At weaning, the mice were genotyped via polymerase chain reaction (PCR) with genomic DNA extracted from ear punch samples. Genomic DNA was isolated according to the protocol from Jackson Laboratory. The primers *Brpf1*-F (5′-GAC TAG GTT GGG ACC TAA GTG TAA A-3′) and *Brpf1*-R (5′-GGC TTC AGA GTT GGC TCT TTA AAT TC-3′) were used to amplify the 345- and 240-bp bands for the targeted and WT allele, respectively. *Cre*-F (5′-CAT ATT GGC AGA ACG AAC GAA ACG C-3′) and *Cre*-R (5′-CCT GTT TCA CTA TCC AGG TTA CGG-3′) were used for detection of a 413-bp fragment of the Cre transgene. A 25 μL PCR reaction was set up with 12.5 μL of premix Taq polymerase, 1.5 μL genomic DNA, 1 μL of each primer (10 pmol/μL), and 9 μL of sterile nuclease-free water. PCR cycling conditions were as follows: 94°C × 3 minutes, 33 PCR cycles (94°C × 30 seconds, 62°C × 35 seconds, and 72°C × 35 seconds), and 72°C × 5 minutes.

Nissl staining

Nissl staining was performed on 3 pairs of 6-month-old WT and cKO mice as previously described (You et al., 2015a). Mice were euthanized via isoflurane inhalation and decapitated. Coronal paraffin sections of brain tissue were dewaxed and rehydrated through a gradient series of ethanol, stained in 0.1% cresyl violet solution (Solarbio Life Sciences, Beijing, China) (prepared with 0.3% glacial acetic acid and filtered) for 10 minutes, rinsed in distilled H_2O, dehydrated in a gradient of ethanol, cleared in xylene, and covered with glass coverslips for examination under a light microscope. Slides were also digitized with a KFpro slide scanner (KFBio, Zhejiang, China) for further analysis.

RNA-Seq and analysis

Total RNA was extracted from the hippocampal CA1 tissues of 4 pairs of 2-month-old WT and cKO mice. The RNA was of high quality with RNA integrity number (RIN) values of more than 9. High-throughput paired-end mRNA sequencing was performed using an Illumina NovaSeq 6000 (Illumina, San Diego, CA, USA) system. For data analysis, the pre-processing sequence was compared with the mouse genome (release-98) via STAR software 2.4.1a (http://github.com/alexdobin/STAR/releases) after removing the linker and low-quality fragments. We used StringTie software 1.2.2 (https://github.com/gpertea/stringtie) to obtain the original sequence counts of known genes, and we calculated the expression of known genes using fragments per kilobase of transcript per million fragments mapped (FPKM). We used DESeq2 software 3.17 (http://www.bioconductor.org/packages/release/bioc/html/DESeq2.html) to screen the differentially expressed genes (DEGs) between the WT and cKO groups (log2 (Fold Change) ≥ 1 or ≤ –1, P value < 0.05). The DEG function was analyzed using the David platform (Huang da et al., 2009) (https://david.ncifcrf.gov/, RRID: SCR_001881), mainly via the Gene Ontology-Biological Process (GO-BP). The raw and processed data were deposited in the Gene Expression Omnibus database with GEO# (GSE212983).

RT-qPCR

We extracted total RNA from hippocampal CA1 tissues from 3 pairs of 2-month-old WT and cKO mice using the Trizol method (Rio et al., 2010). 500 ng of RNA from each of the above samples was reverse-transcribed using the EvoM-MLVRT kit with gDNAClean (Accurate Biotech, Changsha, Hunan Province, China, AG11705), and the resulting cDNA was used as a template for subsequent fluorescent quantitative PCR. RT-qPCR was performed using TB Green Premix Ex Taq (Takara Biomedical Tech., Beijing, China, rr420a). We used the $2^{-\Delta\Delta Ct}$ method (Livak and Schmittgen, 2001) to calculate the relative expression of genes with *Gapdh* as an internal control. The primer sequences were summarized in **Additional Table 1**. The PCR conditions were as follows: 95°C for 30 seconds, 40 cycles of 95°C for 5 seconds and 60°C for 20 seconds.

Electrophysiology

Electrophysiology recordings were performed using brain slices from 3 pairs of 6-month-old WT and cKO mice. Animals were anesthetized with pentobarbital sodium (80 mg/kg; Sigma-Aldrich, Shanghai, China, P3761) and perfused with cold (4°C) glycerol-based modified artificial cerebrospinal fluid containing (in mM) 250 glycerol, 2.5 KCl, 2 $CaCl_2$, 2 $MgCl_2$, 1.25 NaH_2PO_4, 10 4-(2-hydroxyethyl)-1-piperazineethanesulfonic acid, 25 $NaHCO_3$, and 11 Glucose (carbonated with 95% O_2 and 5% CO_2; pH = 7.2; 325 mOsM). Coronal slices (300 μm) containing the CA1 were prepared with a vibratome (Leica Biosystems, Shanghai, China, VT1200S) in glycerol-based modified artificial cerebrospinal fluid. Slices were placed in a holding chamber filled with artificial cerebrospinal fluid containing (in mM) 126 NaCl, 1.6 KCl, 2.4 $CaCl_2$, 1.4 $MgCl_2$, 1.1 NaH_2PO_4, 26 $NaHCO_3$, and 11 glucose (carbonated with 95% O_2 and 5% CO_2; pH = 7.2; 305 mOsM) at 31°C. After a recovery period of at least 1 hour, individual slices were transferred into the recording chamber superfused with artificial cerebrospinal fluid at a flow rate of 2 mL/min.

Whole-cell voltage-clamp recordings of CA1 pyramidal neurons were performed at 31°C. Neurons were visualized via infrared differential interference contrast video microscopy (Olympus, BX51WI). Under microscopy, CA1 pyramidal neurons were identified as a bright dotted curved region positioned beneath the upper left/right cortex on the slices. Patch pipettes (3–5 MΩ) pulled from borosilicate glass capillaries (Sutter Instrument, Novato, CA, USA, P-2000) were filed with (in mM) 117 Cesium methanesulfonate, 20 4-(2-hydroxyethyl)-1-piperazineethanesulfonic acid, 0.4 ethylene glycol tetraacetic acid, 2.8 NaCl, 5 triethylamine, 5 ATP (Mg), 0.5 GTP (Na), and 5 biocytin (pH = 7.2; 275 mOsM). mEPSC recordings were made using a Multiclamp 700B amplifier (Molecular Devices, San Jose, CA, USA), and the data were filtered at 2 kHz and digitized at 20 kHz with the Digidata 1440A (Molecular Devices). The series resistance (10–25 MΩ) was monitored with a 2-mV depolarizing pulse (2 ms) every 2 seconds. mEPSCs were recorded in neurons that were voltage-clamped at -70 mV in the sodium channel blocker tetrodotoxin (0.5 μM; Research Institute of the Aquatic Products of Heibei, Qinhuangdao, China) or picrotoxin (100 μM; Cayman Chemical, Ann Arbor, MI, USA). mEPSCs were collected with a pClamp 10 (Molecular Devices) and analyzed using the Mini60 Mini Analysis Program 6.0.3 (Synaptosoft, Fort Lee, NJ, USA). The detection criteria were set at > 12 pA (at least 2 × root mean squared (rms) noise), < 1.75 ms rise time, and < 4 ms decay time. mEPSCs were recorded for 5–6 minutes and the data from the last 5 minutes were processed for analysis.

Behavioral detection

Mice were handled daily for 3 days before the behavioral tests. The tests were performed between 9 a.m. and 5 p.m. The experimenters were blind to the genotype during tests.

Open-field test

The open-field test was performed with 6 pairs of 2-month-old WT and cKO mice as previously described (Nakamoto et al., 2020; Guo et al., 2023). Each mouse was allowed to freely explore a square open field (40 cm × 40 cm, 40 cm height) over 6 time points in a 30-minute session. A 20 cm × 20 cm area in the center of the 40 cm × 40 cm chamber was defined as the central area. The trajectory, residence time (time that mice stay in a specific area), and number of movements of the mice in this central area were recorded and analyzed using Ethovision XT videotracking software (Noldus Information Technologies, Leesburg, VA, USA). Locomotor activity was assessed by measuring the total distance traveled.

MWM

MWM tests were performed on 7 pairs of 2-month-old WT and cKO mice as previously described (Xian et al., 2021; Cao et al., 2023). The mice were introduced into a circular water-filled tank that was 120 cm in diameter, with visual cues on the tank wall as spatial reference points. The water temperature was maintained at 22.0°C and white non-toxic paint was used to make the water turbid and opaque. The water tank was divided into four equal quadrants via straight lines. A circular platform with a diameter of 10 cm was submerged in the water so that it was 1 cm below the surface. On day 1, mice were placed in the room for at least 30 minutes to familiarize themselves with the environment prior to training. During the training period, each mouse was gently placed in the water with its head facing the wall of the tank. The mouse was given 60 seconds to find the platform, and when it reached the platform, it was considered successful if it was able to stay on the platform for 10 seconds. If the mouse could not find the platform within 60 seconds, it was guided to the platform by the experimenter and allowed to stay on the platform for 10 seconds. Each mouse received 4 trials per day starting in the four different quadrants. On day 8, the mice only performed the trial once with the platform removed as a test of memory retention. Ethovision XT videotracking software was used to track the mice and analyze the data.

Contextual fear conditioning test

The contextual fear conditioning test was performed on seven pairs of 2-month-old WT and cKO mice as previously described (Nakamoto et al., 2020). On day 1, the mice were placed in a dark box and allowed to explore freely for 3 minutes before presentation of a 30-second 90-dB (2800 Hz) tone as acoustic stimulation. During the last 1 second of the acoustic stimulation, the experimenter delivered a 0.3 mA pulse of plantar electrical stimulation. The 30-second acoustic stimulation and subsequent 1-second electrical stimulation pulses served as the acousto-electrical correlation condition, and this was repeated 3 times. After the stimulation, the mice were placed back in their original cages and the dark boxes were cleaned. On day 2, we conducted an environmental associative experiment in which the mice were placed in the same shock chamber used the previous day for 8 minutes, and we recorded the time spent stationary. For the sound signal association experiment, the environment of the chamber was changed (new wallpaper). The mice were placed in the chamber for 3 minutes before presentation of a sound with the same frequency used the previous day (90 dB; 2800 Hz) for 3 minutes. We recorded the time spent stationary before and after the sound stimulus.

Novel object recognition test

We conducted the novel object recognition test on 8 pairs of 2-month-old WT and cKO mice in a square-shaped open field (40 cm × 40 cm × 40 cm) as previously described (Gompers et al., 2017). The task included three sessions: adaption, familiarization, and recognition. For the adaption session, mice were placed in the test room for 60 minutes and then transferred into the open field arena for 10 minutes. For the familiarization session, two identical objects (i.e. A1, A2) were placed on the upper left and lower right sides of the open field. The mice were placed in the test room for 60 minutes and then transferred into the open field arena for 10 minutes to enable familiarization with the two objects. For the recognition session, a formal test was conducted 1 hour after the familiarization session. The object A2 was replaced with a new object (B). Mice were placed in the test room for 60 minutes and then transferred into the open field arena for 5 minutes to enable them to freely explore the familiar and novel objects. The open field arena and surroundings were cleaned with 70% ethanol to remove odors between tests. The familiarization and recognition sessions were video tracked and scored using Ethovision XT software. Object exploration time was defined as the time spent sniffing objects and times when the nose-object distance was 2 cm or less. The discrimination ratio was calculated as the time spent sniffing the novel object divided by the total time spent sniffing the novel and familiar objects.

Repetitive self-grooming test

We examined spontaneous repetitive self-grooming behavior in 7 WT and 8 cKO mice that were 6 months old, as previously described (Ellegood et al., 2021). Each test mouse was placed individually into a standard cage with a size of 46 cm × 23.5 cm × 20 cm. The cages were empty without any bedding to avoid potential competitive behavior. Each mouse was habituated to the cage for 10 minutes and then video recorded for 10 minutes. We scored the cumulative time spent grooming all body regions during the second 10-minute period. The examiners conducting the quantification were blind to the genotype.

Three-chamber social test

The three-chamber social test was performed on 8 pairs of 2-month-old WT and cKO mice and 6 pairs of 6-month-old WT and cKO mice, as previously described (Yang et al., 2011; Bales et al., 2014). The apparatus comprised 3 connected chambers without covers (40 cm × 20 cm × 23 cm). Cylindrical cages with fences (11 cm × 10.5 cm × 1 cm) were placed symmetrically at the corners of the left and right chambers. Manual division of the compartments was provided by circular openings (3.5 cm diameter) in dividing walls made of clear plexiglass. A weighted cup was placed on the top of the cage to prevent the test mouse from climbing. Three zones were defined using the EthoVision XT software, and we measured the amount of time spent in each chamber for each phase of the test. The test mouse was first put in the center chamber for 5 minutes. The entries to the left and right chambers were blocked during this 5-minute habituation session. After habituation, a novel male mouse was put in one of the side chambers. The position of the novel mouse in the left or right chamber was systematically alternated between trials. The test mouse was allowed to explore the apparatus for 10 minutes with the 2 entry doors to the side chambers open. The time spent in each chamber was automatically recorded by the EthoVision XT software.

Statistical analysis

No statistical methods were used to predetermine the sample sizes. However, our sample sizes are similar to those reported in previous publications (Reza-Zaldivar et al., 2019; Wu et al., 2022). No animals or data points were excluded from the analysis. GraphPad Prism version 9.0.0 for Windows (GraphPad Software, San Diego, CA, USA, www.graphpad.com) was used to analyze the data and plot graphs. Our data were subject to the Shapiro-Wilk test to assess normality, and the Student's *t*-test to compare two independent groups. For behavioral tests, a two-way analysis of variance with the Bonferroni *post hoc* test was used to examine statistical differences between the two independent groups. All data are presented as mean ± standard deviation (SD), with statistical significance set at $P < 0.05$. Sample sizes are described in the figure legends. The experimenters were blind to the genotypes.

Results

Forebrain excitatory neuron-specific knockout of *Brpf1* leads to reduced excitatory synaptic transmission

To determine the function of Brpf1 in the mouse postnatal forebrain, we mated *Brpf1*$^{flx/flx}$ mice with CaMKIIa-Cre mice, in which Cre recombinase is specifically expressed in the forebrain, especially in the CA1 pyramidal neurons of the hippocampus and layer V pyramidal neurons of the cerebral cortex, starting in the 3rd to 4th week postnatally (Mayford et al., 1996). The resulting *Brpf1*$^{flx/+}$; CaMKIIa-Cre mice were grossly normal, and further intercrossing yielded *Brpf1*$^{flx/flx}$; CaMKIIa-Cre (cKO) mice. The cKO mice were viable and the knockout efficiency in the hippocampus reached about 60% in 2-month-old mice ($n = 3$ pairs, $P = 0.0003$; **Figure 1A**). We obtained an expected Mendelian ratio for the survival of cKO mice into adulthood after genotyping about 210 offspring from *Brpf1*$^{flx/+}$; *CaMKIIa-Cre* intercrosses, indicating no major postnatal lethality of forebrain excitatory neuron-specific knockout of Brpf1 (**Table 1**). We previously reported that acute 50% knockdown of *Brpf1* did not affect neuronal morphology in primary cultured hippocampal neurons (Xian et al., 2021). Thus, we did not expect neuronal morphological changes in cKO mice at 2 months old, and so checked at a later stage, i.e., 6 months old. Gross histology examination revealed no major morphological abnormalities in the hippocampus or cerebral cortex in 6-month-old cKO mice via Nissl staining ($n = 3$ pairs; **Figure 1B** and **C**).

We previously reported a reduced excitatory synaptic transmission in primary cultured hippocampal neurons upon *Brpf1* knockdown (Xian et al., 2021). To confirm this effect in the context of retained cytoarchitecture and synaptic circuits *in vivo*, we performed whole-cell patch-clamp recordings of CA1 pyramidal neurons in acute brain slices from 3 pairs of 6-month-old WT and cKO mice. We performed electrophysiological recordings on 6-month-old mice to determine whether the electrophysiological features had changed even if the gross morphological features were the same. We found that the frequency but not the amplitude of mEPSCs decreased significantly, suggesting that conditional deletion of *Brpf1* in forebrain excitatory neurons impairs general spontaneous miniature excitatory transmission (representative traces, **Figure 1D**; mEPSC frequency and amplitude, $n = 18$ *vs*. 14 neurons from 3 mice each, $P = 0.0369$ for **Figure 1E** and $P = 0.4733$ for **Figure1F**). To exclude the influence of cell membrane properties, we examined basic membrane properties. Access resistance, membrane resistance, membrane capacitance, and holding currents were unchanged in cKO CA1 pyramidal cells compared with the control, indicating intact general membrane properties in these cells in cKO mice ($n = 19$ *vs*. 14 neurons from 3 mice each, $P = 0.9070$ and 0.3623 for **Figure 1G** and **I**, respectively; $n = 19$ *vs*. 16 neurons from 3 mice each, $P = 0.0580$ for **Figure 1H**; $n = 17$ *vs*. 14 neurons from 3 mice each, $P = 0.5365$ for **Figure 1J**).

Together, these results indicate that conditional deletion of *Brpf1* in forebrain excitatory neurons does not affect cell membrane properties but impairs general miniature excitatory synaptic transmission.

Forebrain excitatory neuron-specific knockout of *Brpf1* leads to impaired spatial reference and contextual fear memory

Patients with BRPF1 mutations showed an almost 100% penetrance of intellectual disability (Xu et al., 2011; Mattioli et al., 2017; Yan et al., 2017, 2020; Pode-Shakked et al., 2019; Zhao et al., 2019; Keywan et al., 2020; Naseer et al., 2020; Souza et al., 2022). To examine the impact of Brpf1 deletion in forebrain excitatory neurons, especially CA1 pyramidal neurons, on learning and memory, we performed a series of cognitive tasks with 7 pairs of 2-month-old WT and cKO mice. Note that we performed the MWM and fear conditioning tests on 6-month-old mice, and found a significant impairment in cKO mice (**Additional Figure 1**). To determine whether this effect occurs at an earlier age, i.e. at 2 months old, we performed most of the behavioral tests on 2-month-old mice. During the spatial memory tests (MWM), mice were trained for 7 days to find a hidden platform fixed in the southwest quadrant, and we conducted a probe trial on day 8 without the hidden platform. cKO mice did not show a significant difference in the latency (time spent) to find the platform compared with WT mice during the 7-day training period, indicating that a deficiency of *Brpf1* does not affect the acquisition of spatial memory (**Figure 2A**). On day 8, the platform was removed and the spatial memory of both groups of mice was tested as they tried to find the hidden platform. WT mice spent significantly longer in the target quadrant

Table 1 | **Genotype distribution among the offspring from Brpf1$^{f/+}$; *CAMK2a-Cre* intercross**

Stage	*Brpf1*$^{f/f}$*;CAMK2a-Cre*	*Brpf1*$^{f/f}$*;WT*	*Brpf1*$^{f/+}$*;CAMK2a-Cre*	*Brpf1*$^{f/+}$*;WT*	*WT;WT*	Total
Dead pri-weaning	1[a], 1[c]	3[b], 1[c]	3[a], 1[b], 3[c], 1[d]	1[b], 2[c]	2[b]	19
Alive post-weaning	50	16	83	22	20	191
Expected Mendelian ratio	3/16	1/16	3/8	1/8	1/16	

a: The pups were dead due to smaller size' b: the pups were eaten by their mother; c: the pups were dead of unknown reasons; d: the pups were dead due to fighting. *Brpf1*: bromodomain and PHD finger containing protein 1; WT: wild type.

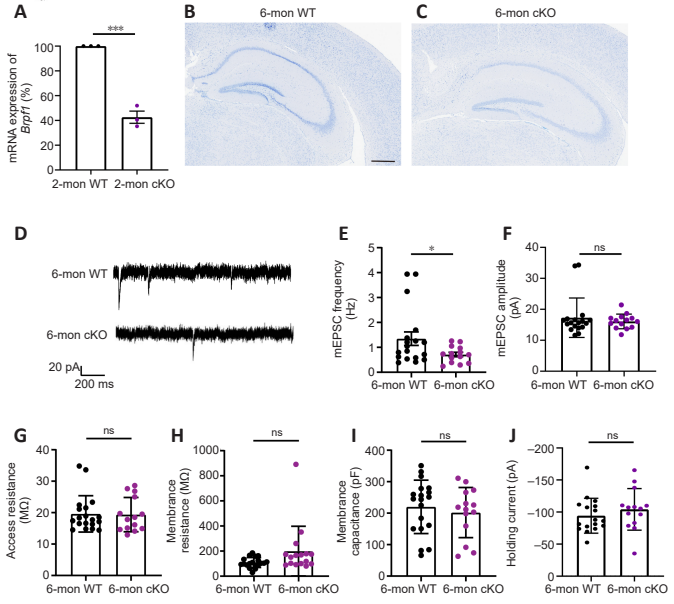

Figure 1 | **Forebrain excitatory neuron-specific knockout of *Brpf1* leads to decreased mEPSC frequency.**

(A) Knockout efficiency of *Brpf1* in the hippocampus from 2-month-old WT and cKO mice via reverse transcription quantitative reverse transcription (n = 3 mice for each group). (B, C) Representative image of Nissl staining on brain coronal sections from 6-month-old WT and cKO mice, respectively (n = 3 mice for each group). No obvious gross morphological changes were observed in the hippocampus between the two groups. Scale bars: 400 μm. (D) Representative traces of mEPSCs in hippocampal CA1 pyramidal neurons from acute brain slices from 6-month-old WT and cKO mice, respectively. Scale of 20 pA and 200 ms is shown. The trace fragments represented signals of 1.5 seconds. (E, F) Statistical comparison of mEPSC frequency and amplitude recorded in CA1 pyramidal neurons from acute brain slices from 3 pairs of 6-month-old WT and cKO mice, respectively (WT: n = 18 neurons and cKO: 14 neurons). (G–J) Statistical comparison of membrane properties including access resistance, membrane resistance, membrane capacitance, and holding current recorded in the same cells as E and F (n = 19 (WT) *vs*. 14 (cKO) neurons for G, I; n = 19 (WT) *vs*. 16 (cKO) neurons for H; n = 17 (WT) *vs*. 14 (cKO) neurons for J). Data are expressed as mean ± SD. *P < 0.05, ***P < 0.001 (Student's t-test). 2-mon: 2-month-old; 6-mon: 6-month-old; *Brpf1*: bromodomain and PHD finger containing protein 1; cKO: conditional knockout; mEPSC: miniature excitatory postsynaptic current; ns: not significant; WT: wild type.

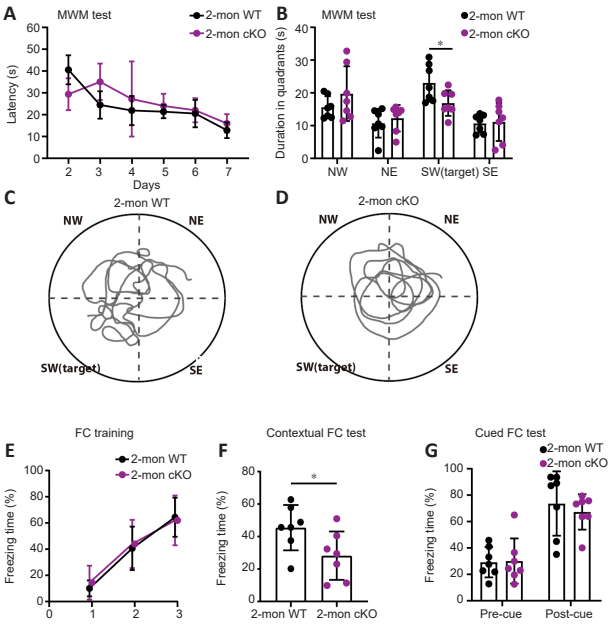

Figure 2 | **Forebrain excitatory neuron-specific knockout of *Brpf1* leads to impaired spatial reference and contextual fear memory.**

(A) Statistical comparison of 2-month-old WT and cKO mice in terms of the latency to reach the hidden platform during a 7-day training period in the MWM test (n = 7 mice for each group). (B) Statistical comparison of the duration spent in each of the 4 quadrants on day 8 for 2-month-old mice in the MWM test (n = 7 mice for each group). (C, D) Representative trajectory image of a 2-month-old WT and cKO mouse on day 8 in the MWM test, respectively. The field was divided into 4 quadrants. (E) Statistical comparison of the percentage of freezing time in 2-month-old WT and cKO mice during the phase of fear memory acquisition in contextual and cued fear conditioning tests (n = 7 mice for each group). (F) Statistical comparison of the percentage of freezing time in 2-month-old WT and cKO mice in a scene fear memory (contextual) test (n = 7 mice for each group). (G) Statistical comparison of the percentage of freezing time in 2-month-old WT and cKO mice in a sound fear memory (cued) test (n = 7 mice for each group). Data are expressed as mean ± SD. *P < 0.05 (two-way analysis of variance with Bonferroni *post hoc* test). *Brpf1*: Bromodomain and PHD finger containing protein 1; cKO: conditional knockout; FC: fear conditioning; MWM: Morris water maze; NE: northeast; NW: northwest; SE: southeast; SW (target): southwest; WT: wild type.

than the other three quadrants, indicating good spatial reference memory. In contrast, cKO mice did not spend longer in the target quadrant than the other 3 quadrants. In addition, cKO mice spent significantly less time in the target quadrant than WT mice (n = 7 pairs, P = 0.0367 for the southwest quadrant in **Figure 2B**; representative trace recordings in **Figure 2C** and **D**). The duration of time spent in the target quadrant decreased significantly from 23.04 to 16.89 seconds. Together, these data suggest that forebrain excitatory neuron-specific deletion of *Brpf1* led to impaired spatial reference memory.

To assess fear in the cKO mice, which is a complicated behavior involving circuits including the hippocampus, cortex, and amygdala (Moustafa et al., 2013; Zelikowsky et al., 2014), we performed contextual and cued fear conditioning. All mice were subjected to conditioned training, environmental correlation, and sound signal correlation. During the first day of fear memory learning, as the length of the acoustoelectric stimuli increased, the freezing time tended to increase in 2-month-old mice of both genotypes, suggesting that both groups acquired fear memory associated with the acoustoelectric stimuli (**Figure 2E**). During the second day, in the fear memory test (contextual), 2-month-old cKO mice exhibited significantly lower freezing time compared with WT mice (n = 7 pairs, P = 0.0451; **Figure 2F**), suggesting impaired contextual fear memory. In the sound conditioned fear memory test (cued), however, there was no significant difference between the WT and cKO mice both during the first 3 minutes of the adaptation phase (pre-cue) and during the session with sound stimulation (post-cue), suggesting a minimal change in cued fear memory formation in 2-month-old cKO mice (n = 7 pairs, P = 0.5971 post-cue; **Figure 2G**). Together, these data indicate that forebrain excitatory neuron-specific deletion of *Brpf1* led to impaired contextual but not cued fear memory, which is consistent with the reported role of the hippocampus in the acquisition of conditioned fear responses to the context but not the cue (Phillips and LeDoux, 1992).

Forebrain excitatory neuron-specific knockout of *Brpf1* has little effect on social ability, repetitive behavior, or locomotor activity

To date, 43 cases of BRPF1 mutations have been reported, confirming a causal role of BRPF1 in intellectual disability. One of these was in an autistic individual (Zu et al., 2022). Here, we examined autism-like behaviors including sociability using the three-chamber social test, cognitive ability using novel object recognition, repetitive behavior via self-grooming, and locomotor activity via the open field test.

The three-chamber test is a typical test for sociability (Gompers et al., 2017). The time spent in the chamber with the novel mouse (stranger) tended to be longer than that in the empty chamber for both groups at 2 and 6 months old, respectively (n = 8 pairs for 2-month-old mice, WT stranger *vs*. WT empty, P = 0.8713, cKO stranger *vs.* cKO empty, P = 0.1102, **Figure 3A**; n = 6 pairs for 6-month-old mice, WT stranger *vs*. WT empty, P = 0.1271, cKO stranger *vs.* cKO empty, P = 0.8704, **Figure 3B**). cKO mice showed no significant difference in sociability compared with WT mice. Cognitive ability was examined using the novel object recognition task. The discrimination ratio of the cKO mice was similar to that of WT mice, suggesting a similar preference for novel objects and memory for familiar objects (n = 8 pairs for 2-month-old mice, P = 0.7370, **Figure 3C**). Moreover, the number of times that cKO mice explored novel objects was not significantly different from that of WT mice (n = 8 pairs for 2-month-old mice, P = 0.5392, **Figure 3D**). Thus, the cKO mice showed no clear differences in memory ability when exploring novel and familiar objects. Self-grooming is a useful measurement of autism-like repetitive behavior (Ellegood et al., 2021). We found no significant differences in repetitive behaviors in the self-grooming assay, indicating that cKO mice showed few signs of autism-like repetitive behavior (n = 7 *vs*. 8 for 6-month-old mice, P = 0.3932, **Figure 3E**). We also tested whether hippocampus-specific deletion of *Brpf1* affected locomotor activity using the open field test. The distance traveled by the cKO mice during each of the 6 time points was not significantly different from that of the WT mice (**Figure 3F**). The total distance traveled and mean velocity of locomotion of the cKO mice were similar to those in the WT mice (n = 6 pairs for 2-month-old mice, P = 0.4281 for **Figure 3G** and P = 0.3611 for **Figure 3H**). Taken together, these results suggest that forebrain excitatory neuron-specific loss of *Brpf1* does not affect sociability, recognition, repetitive behavior, or locomotor activity.

Forebrain excitatory neuron-specific knockout of *Brpf1* leads to dysregulated gene activation and suppression

To investigate the molecular mechanisms underlying the reduced excitatory synaptic transmission and impaired spatial and fear memory following *Brpf1* forebrain excitatory neuron-specific knockout, we extracted total RNA from hippocampal CA1 tissue from 4 pairs of 2-month-old WT and cKO mice for mRNA-Seq analysis. We subjected 177 upregulated genes and 433 downregulated genes to GO-BP analysis (**Figure 4A** and **Additional Table 2**), which revealed that upregulated genes were mainly involved in the Wnt signaling pathway and transcriptional regulation, while downregulated genes were mainly involved in the regulation of the nitric oxide biosynthetic process and immune response (**Figure 4B** and **Additional Table 3**).

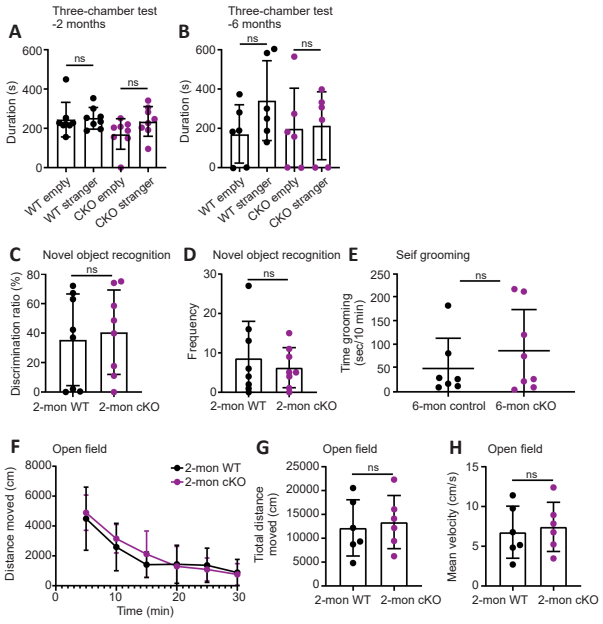

Figure 3 | Forebrain excitatory neuron-specific knockout of *Brpf1* has minimal effect on social ability, repetitive behavior, and locomotor activity.

(A, B) Statistical comparison of duration spent in the chamber with a novel mouse or in the empty chamber between WT and cKO mice using the three-chamber social test, a standard measurement for sociability. We tested 8 pairs of 2-month-old and 6 pairs of 6-month-old mice. (C) Statistical comparison of the percentage of the discrimination ratio for 2-month-old WT and cKO mice in the novel object recognition task (n = 8 pairs). (D) Statistical comparison of the frequency of exploration of new objects in 2-month-old WT and cKO mice in the novel object recognition task (n = 8 pairs). (E) Statistical comparison of time grooming during a 10-minute recording session between 6-month-old WT and cKO mice using an repetitive self-grooming test (n = 7 for WT mice, n = 8 for cKO mice). (F) Statistical comparison of the distance moved for 2-month-old WT and cKO mice over 6 time points in a total 30-minute session in the open field task (n = 6 pairs). (G) Statistical comparison of the total distance moved in 30 minutes for 2-month-old WT and cKO mice in the open field task (n = 6 pairs). (H) Statistical comparison of mean velocity for 2-month-old WT and cKO mice in the open field task (n = 6 pairs). Data are expressed as mean ± SD. Two-way analysis of variance followed by Bonferroni *post hoc* test was used. *Brpf1*: bromodomain and PHD finger containing protein 1; cKO: conditional knockout; ns: not significant; WT: wild type.

To help explain the observed reduction in mEPSC frequency and impairment in spatial and fear memory, we manually examined the 433 downregulated DEGs and found that 16 genes were closely related to neural development, axon guidance, synapse function, and memory (**Table 2**). We selected 10 out of the 16 genes, together with other downregulated and upregulated DEGs, and verified them using three pairs of 2-month-old WT and cKO mice via RT-qPCR (**Figure 4C** and **Additional Table 4**). Because of the difference in measuring the local region (about 200–500 bp) *vs*. full-length region (covering all the exons) of a specific gene via qPCR and RNA-Seq, respectively, the absolute level of fold change may differ. Here, the validation of an upregulation or downregulation trend is more important. The results showed a dual role for *Brpf1* in regulating gene expression, that is, regulating both gene activation and suppression.

Upon conditional deletion of *Brpf1*, we verified the significant downregulation of the protocadherin gamma subfamily B 1 (*Pcdhgb1*), solute carrier family 16 member 7 (*Slc16a7*), roundabout guidance receptor 3 (*Robo3*), and rhodopsin (*Rho*), which are related to neural development and synapse function. *Pcdhgb1* is a subfamily B1 of γ-protocadherin, which can mediate astrocyte-neuron contact and control central nervous system synapse development (Garrett and Weiner, 2009). It has also been implicated in the proper patterning of axon terminals (Peek et al., 2017) and dendritic arborization (Suo et al., 2012). Slc16a7 is the main neuronal monocarboxylate transporter, and it is postsynaptically colocalized with α-amino-3-hydroxy-5-methyl-4-isoxazolepropionic acid receptor at excitatory synapses (Bergersen et al., 2005). It is involved in lactate transport, and is active in Schaffer collateral-CA1 synapses, hippocampal mossy fiber to CA3 synapses, and parallel fiber to Purkinje cell synapses. Neuronal *Slc16a7* is required for hippocampus-dependent spatial information acquisition, retention, and long-term memory formation (Netzahualcoyotzi and Pellerin, 2020). *Robo3*, as a component of the Slit-Robo axis, controls neurite outgrowth and axon guidance (Simpson et al., 2000). *Robo3* deficiency in the auditory system led to ectopic synapses with reduced neurotransmitter release, fewer fast-releasable synaptic vesicles, and smaller presynaptic Ca^{2+} currents (Michalski et al., 2013). *Rho* GTPases are critical for maintaining dendritic spine homeostasis, regulating synaptic transmission and plasticity, and for learning and memory (Zhang et al., 2021). The markedly decreased expression of these genes in cKO mice (**Figure 4C**) is consistent with the electrophysiological and behavioral defects observed. These results indicated that *Brpf1* acts to promote expression of genes related to neural development, synapse function, and memory in the hippocampus.

In terms of validating the upregulated genes, firstly, paired genes like homeodomain 2 (*Pitx2*) and ventral anterior homeobox 2 (*Vax2*), which are related to the Wnt signaling pathway, were markedly upregulated. *Pitx2* is essential for normal development of the mouse subthalamic nucleus and midbrain neurons (Martin et al., 2004). In addition, *Pitx2*-expressing interneurons are the source of cholinergic synapses on spinal and brainstem motor neurons (Zagoraiou et al., 2009; Rozani et al., 2019). The homeodomain protein Vax2 is critical for axial polarization in the eye (Mui et al., 2002, 2005). Thus, *Pitx2* and *Vax2*, 2 transcriptional factors that should not be expressed in the hippocampus, were desuppressed upon Brpf1 deletion. Similarly, transcriptional factor T cell leukemia homeobox 1 (*Tlx1*), paired box 2 (*Pax2*), *Pax1*, twist family BHLH transcription factor 1 (*Twist1*), and POU class 4 homeobox 2 (*Pou4f2*), which are suppressed in the normal brain, were abnormally upregulated. *Tlx1* is involved in the specification of neuronal cell fates (Cheng et al., 2004). *Pax2* regulates the cell fate of GABAergic precursor neurons during cerebellum and spinal cord development. Abnormal expression of *Pax2* could impair the synaptic excitatory-inhibitory balance (Lv et al., 2021). *Pax1* is required for normal development of the skeleton (Wilm et al., 1998). *Twist1* regulates the transcription of genes involved in cranial suture closure, and may also regulate neural tube closure (Bertol et al., 2022). *Pou4f2* may be involved in maintaining visual system neurons (Deng et al., 2014). Finally, homeobox C6 (*Hoxc6*), *Hoxb13*, *Hoxa7*, and *Hoxc9*, which belong to the Hox family of genes and are suppressed in the normal brain, were also upregulated. The *Hox* gene family is involved in axial patterning and normal regionalization of the hindbrain and branchial arches (Parker and Krumlauf, 2020). Such desuppression of transcription factors that are normally not expressed in the hippocampus (**Figure 4C**) is consistent with our previous finding in the dorsal cortex of *Brpf1*$^{flx/flx}$; *Emx1-Cre* mice (You et al., 2015a). These results indicate that *Brpf1* also acts as a silencer to inhibit the expression of genes including the *Wnt* signaling genes, *Hox* genes, and other transcriptional factors in the postnatal forebrain.

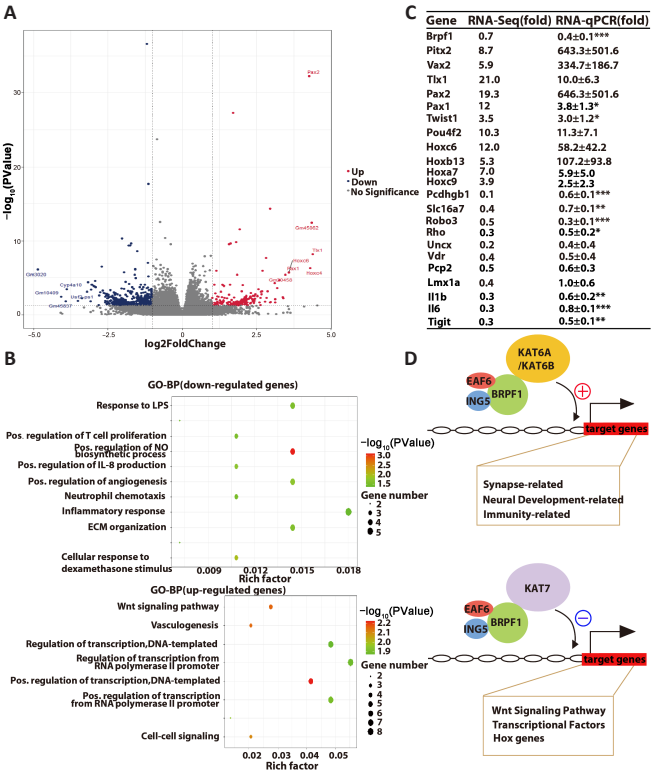

Figure 4 | Forebrain excitatory neuron-specific knockout of *Brpf1* dually dysregulates gene expression.

(A) Volcano plot of DEGs from mRNA sequencing of total RNA from 4 pairs of 2-month-old WT and cKO hippocampal CA1 tissues. Red and blue dots indicate upregulated genes (log_2(fold change) ≥ 1 and P < 0.05) and downregulated genes (log_2(fold change) ≤ –1 and P < 0.05), respectively. (B) Bubble plots represent the GO-BP of downregulated genes (log_2(fold change) ≤ –1 and P < 0.05) and upregulated genes (log_2(fold change) ≥ 1 and P < 0.05) as in A. Dot size reflects gene number, color indicates $-log_{10}P$. (C) The expression of selected genes identified by mRNA sequencing of 4 pairs of 2-month-old WT and cKO hippocampal CA1 tissue was validated by reverse transcription quantitative reverse transcription of 3 pairs of 2-month-old WT and cKO hippocampal CA1 tissue. Fold values indicate the fold change of cKO transcript levels with respect to WT levels. Data are expressed as mean ± SD. *P < 0.05, **P < 0.01, ***P < 0.001 (Student's t-test). (D) Models illustrate the dual role of *Brpf1* in regulating gene expression in the hippocampus. *Brpf1*: bromodomain and PHD finger containing protein 1; cKO: conditional knockout; DEG: differentially expressed genes; GO-BP: gene ontology-biological process; pos.: positive; WT: wild type.

Table 2 | **Selected downregulated genes upon forebrain excitatory neuron-specific knockout of Brpf1 that are related to synapse and neural development**

Gene name	Log_2 (fold change)	*P*-value	Function
Neural development and axon guidance			
Agxt2	–2.494	0.024	Regulates Slit and Robo expression which are critical for axon guidance (Brose et al., 1999).
Uncx	–2.367	0.024	Critical role in midbrain DA neuron differentiation and glutamatergic neurogenesis (Rabe et al., 2012).
Lmx1a	–1.491	0.009	Essential role in DA neuron development (Yan et al., 2011), motor coordination and memory impairments upon KO (Laguna et al., 2015).
Nrtn	–1.052	0.006	Promotes survival of neuronal populations (Dass and Kordower, 2007).
Pcp2	–1.011	0.041	Modulates resting membrane potential of rod bipolar neurons (Xu et al., 2008). Although abundant in purkinje cells but no significant anatomic and behavioural deficits observed in KO mice (Mohn et al., 1997; Vassileva et al., 1997).
Robo3	–1.134	2.00E-18	Conditional KO in the auditory system forced a commissural synapse formed on the wrong side, with reduced transmitter release, fewer fast-releasable vesicles, and smaller presynaptic Ca^{2+} currents (Michalski et al., 2013).
Synapse and memory			
Pcdhgb1	–2.927	2.57E-05	Controls synaptogenesis by mediating neuron-astrocyte contact (Garrett and Weiner, 2009).
Pcdhgb4	–1.633	0.025	Implicates in the proper patterning of axon terminals (Peek et al., 2017) and dendritic arborization (Suo et al., 2012).
Vdr	–1.485	0.046	Crucial to modulate hippocampal learning and memory (Liang et al., 2018), and improve conditioned fear memory (Durk et al., 2014). Paraventricular hypothalamus Vdr loss showed impaired mEPSCs (Beck et al., 2022).
Caps2	–1.18	0.005	Promotes BDNF secretion and crucial for hippocampal GABAergic interneuron network. KO mice showed impaired GABAergic systems including reduced frequency and amplitude of mIPSCs (Shinoda et al., 2011).
Chrne	–2.462	0.004	As part of the cholinergic system receptor subunits for excitatory neurotransmitter acetylcholine, which is strongly involved in memory function (Ferreira-Vieira et al., 2016).
Chat	–2.316	0.007	Local elimination of acetylcholine in medial habenula neurons alters glutamate corelease and presynaptic facilitation (Frahm et al., 2015). Chat produces acetylcholine and can improve learning and memory function (Park et al., 2020).
Slc16a7	–1.486	0.003	Enables symporter activity, involved in lactate transport, active in Schaffer collateral-CA1 synapse, hippocampal mossy fiber to CA3 synapse, and parallel fiber to Purkinje cell synapse. It is also named as *Mct2*, the main neuronal monocarboxylate transporter, postsynaptically co-localized with AMPA receptor at excitatory synapses (Bergersen et al., 2005). Neuronal Mct2 is required for hippocampus-dependent spatial information acquisition, retention, and long-term memory formation (Netzahualcoyotzi and Pellerin, 2020).
Phf24	–1.362	0.041	Locates in the presynaptic terminals, synaptic membranes and cytoplasmic matrix of neuronal soma. It is associated with GABA receptor and may regulate GABAergic synaptic transmission (Numakura et al., 2021). KO rats showed an increased sensitivity to drug induced seizures, elevated spontaneous locomotor activity, and impaired spatial memory (Serikawa et al., 2019).
Npas4	–1.043	0.0004	Controls the number and function of GABAergic inhibitory synapses formed on excitatory neurons in the hippocampus. KO mice are prone to seizures (Lin et al., 2008). Later, *Npas* was further found to regulate excitatory-inhibitory balance of neural circuits. Deletion of *Npas4* in SST neurons reduces functional excitation as decreased mEPSC frequency (Spiegel et al., 2014), required for contextual memory formation in the hippocampus (Weng et al., 2018).
Rho	–1.913	0.042	Critical for maintaining dendritic spine homeostasis, regulating synaptic transmission and plasticity, learning and memory (Zhang et al., 2021).

AMPA: alpha-amino-3-hydroxy-5-methyl-4-isoxazolepropionic acid; BDNF: brain-derived neurotrophic factor; Brpf1: bromodomain and PHD finger containing protein 1; DA: dopaminergic; GABA: gamma-aminobutyric acid; KO: knockout; Mct2: monocarboxylate transporter 2; mEPSC: miniature excitatory postsynaptic current; mIPSC: miniature inhibitory postsynaptic current; Npas4: neuronal PAS domain protein 4; SST: somatostatin.

Discussion

In this study, we identified an important role of Brpf1 in postnatal forebrain excitatory neurons, especially in CA1 pyramidal neurons, via conditional deletion of *Brpf1* in forebrain excitatory neurons using CaMKIIa-Cre. Our findings showed that forebrain excitatory neuron-specific loss of *Brpf1* led to reduced mEPSC frequency, impaired spatial reference and contextual fear memory, and dysregulated pathways such as downregulation of *Pcdhgb1*, *Slc16a7*, *Robo3*, and *Rho*, genes critical for synapse function and memory.

Forebrain excitatory neuron-specific deletion of *Brpf1* led to decreased mEPSC frequency but not amplitude, with little changes in membrane properties including membrane resistance and capacitance, in 6-month-old mice. In our previous study, we observed a similar reduction of mEPSC frequency but not amplitude in adeno-associated virus-shBrpf1 infected primary cultured hippocampal neurons derived from E17–18 hippocampi (Xian et al., 2021). Another team reported that $Brpf1^{flx/+}$; *Emx1-Cre* mice showed a decrease in both the frequency and amplitude of mEPSCs recorded from hippocampal CA1 pyramidal neurons in acute brain slices from 1-month-old mice (Su et al., 2019). Such a discrepancy in the mEPSC amplitude could be caused by the differences in the neuronal types that are conditionally deleted by crossing *Brpf1* floxed mice with *CaMKIIa-Cre* vs. *Emx1-Cre* mice, respectively. A change in mEPSC frequency often indicates presynaptic release probability alternation, whereas a change in mEPSC amplitude often indicates postsynaptic receptor function or/and number alternation. Downregulated genes such as *Robo3*, *Pcdhgb1*, and *Vdr*, as revealed by RNA-Seq and validated by RT-qPCR, could help explain the presynaptic alternations of *Brpf1* cKO mice. Robo3 deletion in the auditory system leads to ectopic synapses with reduced neurotransmitter release, fewer fast-releasable synaptic vesicles, and smaller presynaptic Ca^{2+} currents (Michalski et al., 2013). *Pcdhgb1* is a B1 subfamily of γ-protocadherin, which mediates astrocyte-neuron interaction and controls synaptogenesis (Garrett and Weiner, 2009). Besides, the *Pcdhg* cluster is implicated in proper patterning of axon terminals and dendritic arborization (Peek et al., 2017). *Vdr* loss in the paraventricular hypothalamus led to impaired mEPSCs (Beck et al., 2022). Besides impaired presynaptic release, fewer functional synapses could also contribute to the reduction of mEPSC frequency. However, in our previous study, acute 50% knockdown of *Brpf1* did not affect neuronal dendrite complexity in primary cultured hippocampal neurons (Xian et al., 2021), which suggests that the reduction of mEPSC frequency in cKO mice may not have been caused by fewer functional synapses.

As expected, reduced excitatory synaptic transmission is associated with altered learning and memory, as reflected by impaired spatial reference and contextual fear memory. In our previous studies, global *Brpf1* knockouts died at E9.5 (You et al., 2014) and forebrain-specific *Brpf1* knockouts died around 2–3 weeks postnatally (You et al., 2015a). Thus, they could not be evaluated behaviorally past this age. In this study, $Brpf1^{fl/fl}$; *CaMKIIa-Cre* (cKO) mice were grossly normal and viable, and we were able to evaluate the specific impact of *Brpf1* deletion on postnatal forebrain excitatory neurons using a series of behavioral tasks. We previously reported a trend towards impaired spatial memory using the MWM task following stereo-injected acute knockdown of *Brpf1* in the hippocampal CA1 region of 2–3 month-old mice (Xian et al., 2021). In this study, *Brpf1* was genetically deleted in forebrain excitatory neurons starting 3–4 weeks postnatally. The deletion led to a significant impairment in spatial reference and contextual fear memory. This is consistent with a similar defect of spatial and fear memory found in $Brpf1^{flx/+}$; *Emx1-Cre* mice (Su et al., 2019). Downregulated genes such as *Slc16a7*, *Vdr*, and *Lmx1a*, as revealed by RNA-Seq and validated by RT-qPCR, could help to explain the impaired spatial and fear memory found in *Brpf1* cKO mice. *Slc16a7* is required for hippocampus-dependent spatial information acquisition, retention, and long-term memory formation (Netzahualcoyotzi and Pellerin, 2020). *Vdr* signaling is crucial for the modulation of hippocampal learning and memory (Liang et al., 2018), as well as conditioned fear memory (Durk et al.,

2014). Previously, *Lmx1a* KO led to impaired motor coordination and memory (Laguna et al., 2015). In addition, *Pou4f2*, a gene differentially expressed in cKO mice, has been implicated in visual system neuron maintenance (Badea et al., 2009). In future studies, we hope to conduct a visual acuity test to investigate whether *Brpf1* deficiency affects the visual system. This may account for some of the variability observed in the MWM tests.

We found that *Brpf1* forebrain excitatory neuron-specific loss did not lead to significant changes in sociability, cognitive ability, repetitive behavior, or locomotor activity as assessed by the three-chamber social test, novel object recognition, self-grooming test, and open field assay. As mentioned, only one of 43 patients with BRPF1 mutations was reported to be autistic (Zu et al., 2022). The lack of autism-like behaviors such as impaired sociability and repetitive behavior found in our cKO mice is consistent with the low penetrance of autism found in patients with BRPF1 mutations.

Patients with BRPF1 mutations showed a 100% rate of intellectual disability (Zu et al., 2022). We expected *Brpf1* cKO to lead to significant cognitive impairment and learning deficits such as significant changes in novel object recognition and MWM performance (during training phase). There are at least three possible explanations for why we did not observe these expected results. First, the knockout efficiency of cKO was modest, at about 60% in the hippocampus. Second, the sample size for the behavioral tests was relatively small. Third, the expression of *Brpf1* in other cell types (besides forebrain excitatory neurons) or other brain regions may contribute to the cognitive impairment and learning deficits found in patients.

We noticed that six out of the top nine GO-BP downregulated genes were related to immune responses. Consistent with our findings, Xia et al. (2021) profiled a transcription factor network in primary low-grade glioblastoma and identified a gene set of "markers of inflammation", including *Brpf1*. They demonstrated that *Brpf1* can regulate the inflammatory response by manipulating the nuclear factor kappa B (NF-κB) pathway and explored the relationship between *Brpf1* and inflammatory responses and nervous system tumor growth (Xia et al., 2021). Hagberg et al. (2012) demonstrated that inflammatory responses during fetal and neonatal periods may lead to abnormal neuronal and synaptic development, reduced brain volume, cognitive and behavioral abnormalities, and emotional and psychological health problems. Interestingly, some immune cells and signaling pathways involved in this process are also affected in *Brpf1* cKO mice, such as neutrophil chemotaxis and the NF-κB pathway (Hagberg et al., 2012). *Brpf1* deficiency also downregulates the response to lipopolysaccharide, which is commonly used in neuroinflammation models (Feng et al., 2021). This leads to changes in neuronal function and structure, thereby affecting neuroplasticity and cognitive function (Lecca et al., 2022). Together, these findings strongly support a potential role of Brpf1 in immunity, which could be related to its effect on memory and cognition. Further investigations are needed to explore this possibility.

Besides the down-regulation of gene expression, *Brpf1* deletion markedly up-regulated expression of *Wnt* signaling genes, various *Hox* genes, and multiple transcriptional factors critical for various developmental processes, confirmed by RT-qPCR. Interestingly, such up-regulation was not observed in embryos with global deletion of *Brpf1* (You et al., 2014) or hematopoiesis-specific deficient mice (You et al., 2016), nor in primary cultured hippocampal neurons (Xian et al., 2021) or MGE-derived GABAergic neurons (Cao et al., 2021) with *Brpf1* knockdown, suggesting that the suppressive role of Brpf1 is specific to the hippocampus *in vivo*. This is consistent with our previous report on the silencing role of *Brpf1* on gene expression in the dorsal cortex (You et al., 2015a).

The dual role of *Brpf1* in regulating gene expression in the hippocampus may be based on a model, as illustrated. Accumulating evidence from molecular, animal, and human studies has suggested a transcriptional activator role of *Brpf1* via its interaction with *Kat6a* and *Kat6b*. At the molecular level, Brpf1 is a scaffold and an activator of the *Kat6a*/*Kat6b* complex (Ullah et al., 2008). Indeed, animal studies revealed a similar role of *Brpf1* and *Kat6a* in the skeletal development in fish (Miller et al., 2004; Crump et al., 2006; Laue et al., 2008; Hibiya et al., 2009), brain development in mice (Perez-Campo et al., 2014; You et al., 2015c), and hematopoiesis and leukemogenesis in mice (Katsumoto et al., 2006; Shima et al., 2014; Sheikh et al., 2015, 2016; You et al., 2016; He et al., 2020; Yokoyama, 2022). Also, *Brpf1* or *KAT6b* deficiency was associated with similar phenotypes in brain development (Thomas et al., 2000; Thomas and Voss, 2004; Merson et al., 2006; Kraft et al., 2011; Sheikh et al., 2012; You et al., 2015a, c). BRPF1 or KAT6/KAT6B mutations in humans have both been reported in neurodevelopmental disorders with intellectual disability (Zu et al., 2022). All these data support the hypothesis regarding the role of *Brpf1* as a transcriptional activator through *Kat6a*/*Kat6b*. Thus, in the current study, *Brpf1* may act as an activator via *KAT6a*/*Kat6b* to promote the expression of genes related to neural development, synapse, and memory in the hippocampus. Interestingly, the suppressive role of Brpf1 in hippocampal *Hox* gene expression is consistent with the pivotal role of the drosophila *Kat7* ortholog Chameau in *Hox* gene silencing (Grienenberger et al., 2002), indicating that *Brpf1* may work together with *Kat7* as a gene silencer. Thus, B*rpf1* may also act as a silencer via *Kat7* to inhibit the expression of Wnt signaling genes, Hox genes, and other transcriptional factors in the hippocampus. Whether *Brpf1* can function through other partners awaits further investigation.

There are several limitations to our study. First, the sample size used for the behavioral tests was relatively small and should be increased in future work to confirm the role of *Brpf1* in social ability and cognition. In addition, in future studies, molecular profiling should be conducted immediately after specific behavioral tests to explore the association between molecular changes and behaviors.

In summary, our findings showed that forebrain excitatory neuron-specific loss of *Brpf1* led to reduced mEPSC frequency, impaired spatial and fear memory, and dysregulated gene expression such as downregulation of *Pcdhgb1*, *Slc16a7*, *Robo3*, and *Rho* genes critical for synapse and memory. These data help explain intellectual disability in patients with BRPF1 mutations.

Acknowledgments: *We use BioRender.com to create the Graphical abstract.*
Author contributions: *Conceptulization, project supervision and writing-review and editing: LY; most of the experimental carried out: BZ, HZ, YL; validation by RT-qPCR: GZ; mEPSC measurement: YZ, SL; assistence in behavioral tasks: JH; writing-original draft preparation: BZ, HZ, YL; funding acquisition: LY. All authors have read and approved the final version of the manuscript.*
Conflicts of interest: *The authors declare no competing interests.*
Data availability statement: *The raw and processed data of RNA sequencing were deposited in the Gene Expression Omnibus database (GSE212983). Other data relevant to the study are included in the article or uploaded as Additional files.*

Open peer reviewers: *Elisabetta Coppi, University of Florence, Italy; Nathan R Strogulski, The University of Dublin Trinity College, Ireland.*
Additional files:
Additional Table 1: *Primer sequence information of RT-qPCR.*
Additional Table 2: *The differentially expressed gene (DEG) list of 2-month-old cKO vs. WT hippocampal CA1 tissue by mRNA sequencing.*
Additional Table 3: *GO-BP of upregulated and downregulated DEGs of 2-month-old cKO vs. WT hippocampal CA1 tissue by mRNA sequencing.*
Additional Table 4: *The selected DEGs from RNA-Seq validated by RT-qPCR.*
Additional Figure 1: *Morris water maze and fear conditioning test results in 6-month-old WT and cKO mice.*
Additional file 1: *Open peer review reports 1 and 2.*

References

Alkhateeb A, Alazaizeh W (2019) A novel de novo frameshift mutation in KAT6A identified by whole exome sequencing. J Pediatr Genet 8:10-14.

Badea TC, Cahill H, Ecker J, Hattar S, Nathans J (2009) Distinct roles of transcription factors brn3a and brn3b in controlling the development, morphology, and function of retinal ganglion cells. Neuron 61:852-864.

Bae S, Yang A, Kim J, Lee HJ, Park HK (2021) Identification of a novel KAT6A variant in an infant presenting with facial dysmorphism and developmental delay: a case report and literature review. BMC Med Genomics 14:297.

Bales KL, Solomon M, Jacob S, Crawley JN, Silverman JL, Larke RH, Sahagun E, Puhger KR, Pride MC, Mendoza SP (2014) Long-term exposure to intranasal oxytocin in a mouse autism model. Transl Psychiatry 4:e480.

Beck J, da Silva Teixeira S, Harrison K, Phillips G, He Y, Sisley S (2022) Paraventricular vitamin D receptors are required for glucose tolerance in males but not females. Front Endocrinol (Lausanne) 13:869678.

Bergersen LH, Magistretti PJ, Pellerin L (2005) Selective postsynaptic co-localization of MCT2 with AMPA receptor GluR2/3 subunits at excitatory synapses exhibiting AMPA receptor trafficking. Cereb Cortex 15:361-370.

Bertol JW, Johnston S, Ahmed R, Xie VK, Hubka KM, Cruz L, Nitschke L, Stetsiv M, Goering JP, Nistor P, Lowell S, Hoskens H, Claes P, Weinberg SM, Saadi I, Farach-Carson MC, Fakhouri WD (2022) TWIST1 interacts with β/δ-catenins during neural tube development and regulates fate transition in cranial neural crest cells. Development 149:dev200068.

Brea-Fernández A, Dacruz D, Eirís J, Barros F, Carracedo Á (2019) Novel truncating variants expand the phenotypic spectrum of KAT6B-related disorders. Am J Med Genet A 179:290-294.

Brose K, Bland KS, Wang KH, Arnott D, Henzel W, Goodman CS, Tessier-Lavigne M, Kidd T (1999) Slit proteins bind Robo receptors and have an evolutionarily conserved role in repulsive axon guidance. Cell 96:795-806.

Cao J, Xian W, Palihati M, Zhu Y, Wang G, Xie Y, Zhou G, You L (2021) Deficiency of intellectual disability-related gene Brpf1 reduced inhibitory neurotransmission in MGE-derived GABAergic interneurons. G3 (Bethesda) 11:jkab090.

Cao XW, Yang H, Liu XM, Lou SY, Kong LP, Rong LQ, Shan JJ, Xu Y, Zhang QX (2023) Blocking postsynaptic density-93 binding to C-X3-C motif chemokine ligand 1 promotes microglial phenotypic transformation during acute ischemic stroke. Neural Regen Res 18:1033-1039.

Cheng L, Arata A, Mizuguchi R, Qian Y, Karunaratne A, Gray PA, Arata S, Shirasawa S, Bouchard M, Luo P, Chen CL, Busslinger M, Goulding M, Onimaru H, Ma Q (2004) Tlx3 and Tlx1 are post-mitotic selector genes determining glutamatergic over GABAergic cell fates. Nat Neurosci 7:510-517.

Crump JG, Swartz ME, Eberhart JK, Kimmel CB (2006) Moz-dependent Hox expression controls segment-specific fate maps of skeletal precursors in the face. Development 133:2661-2669.

Dass B, Kordower JH (2007) Gene therapy approaches for the treatment of Parkinson's disease. Handb Clin Neurol 84:291-304.

Deng M, Yang H, Xie X, Liang G, Gan L (2014) Comparative expression analysis of POU4F1, POU4F2 and ISL1 in developing mouse cochleovestibular ganglion neurons. Gene Expr Patterns 15:31-37.

Durk MR, Han K, Chow EC, Ahrens R, Henderson JT, Fraser PE, Pang KS (2014) 1α,25-Dihydroxyvitamin D3 reduces cerebral amyloid-β accumulation and improves cognition in mouse models of Alzheimer's disease. J Neurosci 34:7091-7101.

Efthymiou S, Salpietro V, Bettencourt C, Houlden H (2018) Paroxysmal movement disorder and epilepsy caused by a de novo truncating mutation in KAT6A. J Pediatr Genet 7:114-116.

Ellegood J, Petkova SP, Kinman A, Qiu LR, Adhikari A, Wade AA, Fernandes D, Lindenmaier Z, Creighton A, Nutter LMJ, Nord AS, Silverman JL, Lerch JP (2021) Neuroanatomy and behavior in mice with a haploinsufficiency of AT-rich interactive domain 1B (ARID1B) throughout development. Mol Autism 12:25.

Feng X, Zhan F, Luo D, Hu J, Wei G, Hua F, Xu G (2021) LncRNA 4344 promotes NLRP3-related neuroinflammation and cognitive impairment by targeting miR-138-5p. Brain Behav Immun 98:283-298.

Ferreira-Vieira TH, Guimaraes IM, Silva FR, Ribeiro FM (2016) Alzheimer's disease: targeting the cholinergic system. Curr Neuropharmacol 14:101-115.

Frahm S, Antolin-Fontes B, Görlich A, Zander JF, Ahnert-Hilger G, Ibañez-Tallon I (2015) An essential role of acetylcholine-glutamate synergy at habenular synapses in nicotine dependence. Elife 4:e11396.

Garrett AM, Weiner JA (2009) Control of CNS synapse development by {gamma}-protocadherin-mediated astrocyte-neuron contact. J Neurosci 29:11723-11731.

Gompers AL, Su-Feher L, Ellegood J, Copping NA, Riyadh MA, Stradleigh TW, Pride MC, Schaffler MD, Wade AA, Catta-Preta R, Zdilar I, Louis S, Kaushik G, Mannion BJ, Plajzer-Frick I, Afzal V, Visel A, Pennacchio LA, Dickel DE, Lerch JP, et al. (2017) Germline Chd8 haploinsufficiency alters brain development in mouse. Nat Neurosci 20:1062-1073.

Grienenberger A, Miotto B, Sagnier T, Cavalli G, Schramke V, Geli V, Mariol MC, Berenger H, Graba Y, Pradel J (2002) The MYST domain acetyltransferase Chameau functions in epigenetic mechanisms of transcriptional repression. Curr Biol 12:762-766.

Guo Y, Wang YY, Sun TT, Xu JJ, Yang P, Ma CY, Guan WJ, Wang CJ, Liu GF, Liu CQ (2023) Neural progenitor cells derived from fibroblasts induced by small molecule compounds under hypoxia for treatment of Parkinson's disease in rats. Neural Regen Res 18:1090-1098.

Hagberg H, Gressens P, Mallard C (2012) Inflammation during fetal and neonatal life: implications for neurologic and neuropsychiatric disease in children and adults. Ann Neurol 71:444-457.

He Q, Hong M, He J, Chen W, Zhao M, Zhao W (2020) Isoform-specific involvement of Brpf1 in expansion of adult hematopoietic stem and progenitor cells. J Mol Cell Biol 12:359-371.

Hibiya K, Katsumoto T, Kondo T, Kitabayashi I, Kudo A (2009) Brpf1, a subunit of the MOZ histone acetyl transferase complex, maintains expression of anterior and posterior Hox genes for proper patterning of craniofacial and caudal skeletons. Dev Biol 329:176-190.

Huang da W, Sherman BT, Lempicki RA (2009) Bioinformatics enrichment tools: paths toward the comprehensive functional analysis of large gene lists. Nucleic Acids Res 37:1-13.

Jiang M, Yang L, Wu J, Xiong F, Li J (2021) A de novo heterozygous variant in KAT6A is associated with a newly named neurodevelopmental disorder Arboleda-Tham syndrome-a case report. Transl Pediatr 10:1748-1754.

Katsumoto T, Aikawa Y, Iwama A, Ueda S, Ichikawa H, Ochiya T, Kitabayashi I (2006) MOZ is essential for maintenance of hematopoietic stem cells. Genes Dev 20:1321-1330.

Kennedy J, Goudie D, Blair E, Chandler K, Joss S, McKay V, Green A, Armstrong R, Lees M, Kamien B, Hopper B, Tan TY, Yap P, Stark Z, Okamoto N, Miyake N, Matsumoto N, Macnamara E, Murphy JL, McCormick E, et al. (2019) KAT6A Syndrome: genotype-phenotype correlation in 76 patients with pathogenic KAT6A variants. Genet Med 21:850-860.

Keywan C, Holm IA, Poduri A, Brownstein CA, Alexandrescu S, Chen J, Geffre C, Goldstein RD (2020) A de novo BRPF1 variant in a case of Sudden Unexplained Death in Childhood. Eur J Med Genet 63:104002.

Korakavi N, Bupp C, Grysko B, Juusola J, Borta C, Madura C (2022) First case of pan-suture craniosynostosis due to de novo mosaic KAT6A mutation. Childs Nerv Syst 38:173-177.

Kraft M, Cirstea IC, Voss AK, Thomas T, Goehring I, Sheikh BN, Gordon L, Scott H, Smyth GK, Ahmadian MR, Trautmann U, Zenker M, Tartaglia M, Ekici A, Reis A, Dörr HG, Rauch A, Thiel CT (2011) Disruption of the histone acetyltransferase MYST4 leads to a Noonan syndrome-like phenotype and hyperactivated MAPK signaling in humans and mice. J Clin Invest 121:3479-3491.

Laguna A, Schintu N, Nobre A, Alvarsson A, Volakakis N, Jacobsen JK, Gómez-Galán M, Sopova E, Joodmardi E, Yoshitake T, Deng Q, Kehr J, Ericson J, Svenningsson P, Shupliakov O, Perlmann T (2015) Dopaminergic control of autophagic-lysosomal function implicates Lmx1b in Parkinson's disease. Nat Neurosci 18:826-835.

Laue K, Daujat S, Crump JG, Plaster N, Roehl HH, Tübingen 2000 Screen Consortium, Kimmel CB, Schneider R, Hammerschmidt M (2008) The multidomain protein Brpf1 binds histones and is required for Hox gene expression and segmental identity. Development 135:1935-1946.

Lecca D, Jung YJ, Scerba MT, Hwang I, Kim YK, Kim S, Modrow S, Tweedie D, Hsueh SC, Liu D, Luo W, Glotfelty E, Li Y, Wang JY, Luo Y, Hoffer BJ, Kim DS, McDevitt RA, Greig NH (2022) Role of chronic neuroinflammation in neuroplasticity and cognitive function: A hypothesis. Alzheimers Dement 18:2327-2340.

Liang Q, Cai C, Duan D, Hu X, Hua W, Jiang P, Zhang L, Xu J, Gao Z (2018) Postnatal vitamin D intake modulates hippocampal learning and memory in adult mice. Front Neurosci 12:141.

Lin Y, Bloodgood BL, Hauser JL, Lapan AD, Koon AC, Kim TK, Hu LS, Malik AN, Greenberg ME (2008) Activity-dependent regulation of inhibitory synapse development by Npas4. Nature 455:1198-1204.

Lin YF, Lin TC, Kirby R, Weng HY, Liu YM, Niu DM, Tsai SF, Yang CF (2020) Diagnosis of Arboleda-Tham syndrome by whole genome sequencing in an Asian boy with severe developmental delay. Mol Genet Metab Rep 25:100686.

Livak KJ, Schmittgen TD (2001) Analysis of relative gene expression data using real-time quantitative PCR and the 2(-Delta Delta C(T)) method. Methods 25:402-408.

Lv N, Wang Y, Zhao M, Dong L, Wei H (2021) The role of PAX2 in neurodevelopment and disease. Neuropsychiatr Dis Treat 17:3559-3567.

Marji FP, Hall JA, Anstadt E, Madan-Khetarpal S, Goldstein JA, Losee JE (2021) A novel frameshift mutation in KAT6A is associated with pancraniosynostosis. J Pediatr Genet 10:81-84.

Martin DM, Skidmore JM, Philips ST, Vieira C, Gage PJ, Condie BG, Raphael Y, Martinez S, Camper SA (2004) PITX2 is required for normal development of neurons in the mouse subthalamic nucleus and midbrain. Dev Biol 267:93-108.

Mattioli F, Schaefer E, Magee A, Mark P, Mancini GM, Dieterich K, Von Allmen G, Alders M, Coutton C, van Slegtenhorst M, Vieville G, Engelen M, Cobben JM, Juusola J, Pujol A, Mandel JL, Piton A (2017) Mutations in histone acetylase modifier BRPF1 cause an autosomal-dominant form of intellectual disability with associated ptosis. Am J Hum Genet 100:105-116.

Mayford M, Bach ME, Huang YY, Wang L, Hawkins RD, Kandel ER (1996) Control of memory formation through regulated expression of a CaMKII transgene. Science 274:1678-1683.

Merson TD, Dixon MP, Collin C, Rietze RL, Bartlett PF, Thomas T, Voss AK (2006) The transcriptional coactivator Querkopf controls adult neurogenesis. J Neurosci 26:11359-11370.

Michalski N, Babai N, Renier N, Perkel DJ, Chédotal A, Schneggenburger R (2013) Robo3-driven axon midline crossing conditions functional maturation of a large commissural synapse. Neuron 78:855-868.

Miller CT, Maves L, Kimmel CB (2004) moz regulates Hox expression and pharyngeal segmental identity in zebrafish. Development 131:2443-2461.

Mohn AR, Feddersen RM, Nguyen MS, Koller BH (1997) Phenotypic analysis of mice lacking the highly abundant Purkinje cell- and bipolar neuron-specific PCP2 protein. Mol Cell Neurosci 9:63-76.

Moustafa AA, Gilbertson MW, Orr SP, Herzallah MM, Servatius RJ, Myers CE (2013) A model of amygdala-hippocampal-prefrontal interaction in fear conditioning and extinction in animals. Brain Cogn 81:29-43.

Mui SH, Kim JW, Lemke G, Bertuzzi S (2005) Vax genes ventralize the embryonic eye. Genes Dev 19:1249-1259.

Mui SH, Hindges R, O'Leary DD, Lemke G, Bertuzzi S (2002) The homeodomain protein Vax2 patterns the dorsoventral and nasotemporal axes of the eye. Development 129:797-804.

Nakamoto C, Kawamura M, Nakatsukasa E, Natsume R, Takao K, Watanabe M, Abe M, Takeuchi T, Sakimura K (2020) GluD1 knockout mice with a pure C57BL/6N background show impaired fear memory, social interaction, and enhanced depressive-like behavior. PLoS One 15:e0229288.

Naseer MI, Abdulkareem AA, Guzmán-Vega FJ, Arold ST, Pushparaj PN, Chaudhary AG, AlQahtani MH (2020) Novel missense variant in heterozygous state in the BRPF1 gene leading to intellectual developmental disorder with dysmorphic facies and ptosis. Front Genet 11:368.

Netzahualcoyotzi C, Pellerin L (2020) Neuronal and astroglial monocarboxylate transporters play key but distinct roles in hippocampus-dependent learning and memory formation. Prog Neurobiol 194:101888.

Numakura Y, Uemura R, Tanaka M, Izawa T, Yamate J, Kuramoto T, Kaneko T, Mashimo T, Yamamoto T, Serikawa T, Kuwamura M (2021) PHF24 is expressed in the inhibitory interneurons in rats. Exp Anim 70:137-143.

Park D, Choi EK, Cho TH, Joo SS, Kim YB (2020) Human neural stem cells encoding ChAT gene restore cognitive function via acetylcholine synthesis, Aβ elimination, and neuroregeneration in APPswe/PS1dE9 mice. Int J Mol Sci 21:3958.

Parker HJ, Krumlauf R (2020) A Hox gene regulatory network for hindbrain segmentation. Curr Top Dev Biol 139:169-203.

Peek SL, Mah KM, Weiner JA (2017) Regulation of neural circuit formation by protocadherins. Cell Mol Life Sci 74:4133-4157.

Perez-Campo FM, Costa G, Lie ALM, Stifani S, Kouskoff V, Lacaud G (2014) MOZ-mediated repression of p16(INK) (4) (a) is critical for the self-renewal of neural and hematopoietic stem cells. Stem Cells 32:1591-1601.

Phillips RG, LeDoux JE (1992) Differential contribution of amygdala and hippocampus to cued and contextual fear conditioning. Behav Neurosci 106:274-285.

Pode-Shakked N, Barel O, Pode-Shakked B, Eliyahu A, Singer A, Nayshool O, Kol N, Raas-Rothschild A, Pras E, Shohat M (2019) BRPF1-associated intellectual disability, ptosis, and facial dysmorphism in a multiplex family. Mol Genet Genomic Med 7:e665.

Rabe TI, Griesel G, Blanke S, Kispert A, Leitges M, van der Zwaag B, Burbach JP, Varoqueaux F, Mansouri A (2012) The transcription factor Uncx4.1 acts in a short window of midbrain dopaminergic neuron differentiation. Neural Dev 7:39.

Reza-Zaldivar EE, Hernández-Sapiéns MA, Gutiérrez-Mercado YK, Sandoval-Ávila S, Gomez-Pinedo U, Márquez-Aguirre AL, Vázquez-Méndez E, Padilla-Camberos E, Canales-Aguirre AA (2019) Mesenchymal stem cell-derived exosomes promote neurogenesis and cognitive function recovery in a mouse model of Alzheimer's disease. Neural Regen Res 14:1626-1634.

Rio DC, Ares M, Jr., Hannon GJ, Nilsen TW (2010) Purification of RNA using TRIzol (TRI reagent). Cold Spring Harb Protoc 2010:pdb.prot5439.

Rozani I, Tsapara G, Witts EC, Deaville SJ, Miles GB, Zagoraiou L (2019) Pitx2 cholinergic interneurons are the source of C bouton synapses on brainstem motor neurons. Sci Rep 9:4936.

Serikawa T, Kunisawa N, Shimizu S, Kato M, Alves Iha H, Kinboshi M, Nishikawa H, Shirakawa Y, Voigt B, Nakanishi S, Kuramoto T, Kaneko T, Yamamoto T, Mashimo T, Sasa M, Ohno Y (2019) Increased seizure sensitivity, emotional defects and cognitive impairment in PHD finger protein 24 (Phf24)-null rats. Behav Brain Res 369:111922.

Sheikh BN, Dixon MP, Thomas T, Voss AK (2012) Querkopf is a key marker of self-renewal and multipotency of adult neural stem cells. J Cell Sci 125:295-309.

Sheikh BN, Yang Y, Schreuder J, Nilsson SK, Bilardi R, Carotta S, McRae HM, Metcalf D, Voss AK, Thomas T (2016) MOZ (KAT6A) is essential for the maintenance of classically defined adult hematopoietic stem cells. Blood 128:2307-2318.

Sheikh BN, Lee SC, El-Saafin F, Vanyai HK, Hu Y, Pang SH, Grabow S, Strasser A, Nutt SL, Alexander WS, Smyth GK, Voss AK, Thomas T (2015) MOZ regulates B-cell progenitors and, consequently, Moz haploinsufficiency dramatically retards MYC-induced lymphoma development. Blood 125:1910-1921.

Shima H, Yamagata K, Aikawa Y, Shino M, Koseki H, Shimada H, Kitabayashi I (2014) Bromodomain-PHD finger protein 1 is critical for leukemogenesis associated with MOZ-TIF2 fusion. Int J Hematol 99:21-31.

Shinoda Y, Sadakata T, Nakao K, Katoh-Semba R, Kinameri E, Furuya A, Yanagawa Y, Hirase H, Furuichi T (2011) Calcium-dependent activator protein for secretion 2 (CAPS2) promotes BDNF secretion and is critical for the development of GABAergic interneuron network. Proc Natl Acad Sci U S A 108:373-378.

Simpson JH, Bland KS, Fetter RD, Goodman CS (2000) Short-range and long-range guidance by Slit and its Robo receptors: a combinatorial code of Robo receptors controls lateral position. Cell 103:1019-1032.

Souza J, do Valle DA, Santos M, Colomé FB, Teive HAG, da Silva Freitas R, Herai RH (2022) BRPF1-associated syndrome: A patient with congenital ptosis, neurological findings, and normal intellectual development. Am J Med Genet A 188:1875-1880.

Spiegel I, Mardinly AR, Gabel HW, Bazinet JE, Couch CH, Tzeng CP, Harmin DA, Greenberg ME (2014) Npas4 regulates excitatory-inhibitory balance within neural circuits through cell-type-specific gene programs. Cell 157:1216-1229.

Su Y, Liu J, Yu B, Ba R, Zhao C (2019) Brpf1 haploinsufficiency impairs dendritic arborization and spine formation, leading to cognitive deficits. Front Cell Neurosci 13:249.

Suo L, Lu H, Ying G, Capecchi MR, Wu Q (2012) Protocadherin clusters and cell adhesion kinase regulate dendrite complexity through Rho GTPase. J Mol Cell Biol 4:362-376.

Thomas T, Voss AK (2004) Querkopf, a histone acetyltransferase, is essential for embryonic neurogenesis. Front Biosci 9:24-31.

Thomas T, Voss AK, Chowdhury K, Gruss P (2000) Querkopf, a MYST family histone acetyltransferase, is required for normal cerebral cortex development. Development 127:2537-2548.

Trinh J, Hüning I, Yüksel Z, Baalmann N, Imhoff S, Klein C, Rolfs A, Gillessen-Kaesbach G, Lohmann K (2018) A KAT6A variant in a family with autosomal dominantly inherited microcephaly and developmental delay. J Hum Genet 63:997-1001.

Ullah M, Pelletier N, Xiao L, Zhao SP, Wang K, Degerny C, Tahmasebi S, Cayrou C, Doyon Y, Goh SL, Champagne N, Côté J, Yang XJ (2008) Molecular architecture of quartet MOZ/MORF histone acetyltransferase complexes. Mol Cell Biol 28:6828-6843.

Urreizti R, Lopez-Martin E, Martinez-Monseny A, Pujadas M, Castilla-Vallmanya L, Pérez-Jurado LA, Serrano M, Natera-de Benito D, Martínez-Delgado B, Posada-de-la-Paz M, Alonso J, Marin-Reina P, O'Callaghan M, Grinberg D, Bermejo-Sánchez E, Balcells S (2020) Five new cases of syndromic intellectual disability due to KAT6A mutations: widening the molecular and clinical spectrum. Orphanet J Rare Dis 15:44.

Vassileva G, Smeyne RJ, Morgan JI (1997) Absence of neuroanatomical and behavioral deficits in L7/pcp-2-null mice. Brain Res Mol Brain Res 46:333-337.

Weng FJ, Garcia RI, Lutzu S, Alviña K, Zhang Y, Dushko M, Ku T, Zemoura K, Rich D, Garcia-Dominguez D, Hung M, Yelhekar TD, Sørensen AT, Xu W, Chung K, Castillo PE, Lin Y (2018) Npas4 is a critical regulator of learning-induced plasticity at mossy fiber-CA3 synapses during contextual memory formation. Neuron 97:1137-1152.e5.

Wilm B, Dahl E, Peters H, Balling R, Imai K (1998) Targeted disruption of Pax1 defines its null phenotype and proves haploinsufficiency. Proc Natl Acad Sci U S A 95:8692-8697.

Wu MY, Zou WJ, Yu P, Yang Y, Li SJ, Liu Q, Xie J, Chen SQ, Lin WJ, Tang Y (2022) Cranial irradiation impairs intrinsic excitability and synaptic plasticity of hippocampal CA1 pyramidal neurons with implications for cognitive function. Neural Regen Res 17:2253-2259.

Xia M, Chen H, Chen T, Xue P, Dong X, Lin Y, Ma D, Zhou W, Shi W, Li H (2021) Transcriptional networks identify BRPF1 as a potential drug target based on inflammatory signature in primary lower-grade gliomas. Front Oncol 11:766656.

Xian W, Cao J, Yuan X, Wang G, Jin Q, Zhang H, Zhou G, You L (2021) Deficiency of intellectual disability-related Gene Brpf1 attenuated hippocampal excitatory synaptic transmission and impaired spatial learning and memory ability. Front Cell Dev Biol 9:711792.

Xu B, Roos JL, Dexheimer P, Boone B, Plummer B, Levy S, Gogos JA, Karayiorgou M (2011) Exome sequencing supports a de novo mutational paradigm for schizophrenia. Nat Genet 43:864-868.

Xu Y, Sulaiman P, Feddersen RM, Liu J, Smith RG, Vardi N (2008) Retinal ON bipolar cells express a new PCP2 splice variant that accelerates the light response. J Neurosci 28:8873-8884.

Yan CH, Levesque M, Claxton S, Johnson RL, Ang SL (2011) Lmx1a and lmx1b function cooperatively to regulate proliferation, specification, and differentiation of midbrain dopaminergic progenitors. J Neurosci 31:12413-12425.

Yan K, Rousseau J, Machol K, Cross LA, Agre KE, Gibson CF, Goverde A, Engleman KL, Verdin H, De Baere E, Potocki L, Zhou D, Cadieux-Dion M, Bellus GA, Wagner MD, Hale RJ, Esber N, Riley AF, Solomon BD, Cho MT, et al. (2020) Deficient histone H3 propionylation by BRPF1-KAT6 complexes in neurodevelopmental disorders and cancer. Sci Adv 6:eaax0021.

Yan K, Rousseau J, Littlejohn RO, Kiss C, Lehman A, Rosenfeld JA, Stumpel CTR, Stegmann APA, Robak L, Scaglia F, Nguyen TTM, Fu H, Ajeawung NF, Camurri MV, Li L, Gardham A, Panis B, Almannai M, Sacoto MJG, Baskin B, et al. (2017) Mutations in the chromatin regulator gene BRPF1 cause syndromic intellectual disability and deficient histone acetylation. Am J Hum Genet 100:91-104.

Yang M, Silverman JL, Crawley JN (2011) Automated three-chambered social approach task for mice. Curr Protoc Neurosci Chapter 8:Unit 8.26.

Yokoyama A (2022) Role of the MOZ/MLL-mediated transcriptional activation system for self-renewal in normal hematopoiesis and leukemogenesis. FEBS J 289:7987-8002.

You L, Chen L, Penney J, Miao D, Yang XJ (2014) Expression atlas of the multivalent epigenetic regulator Brpf1 and its requirement for survival of mouse embryos. Epigenetics 9:860-872.

You L, Zou J, Zhao H, Bertos NR, Park M, Wang E, Yang XJ (2015a) Deficiency of the chromatin regulator BRPF1 causes abnormal brain development. J Biol Chem 290:7114-7129.

You L, Yan K, Zou J, Zhao H, Bertos NR, Park M, Wang E, Yang XJ (2015b) The chromatin regulator Brpf1 regulates embryo development and cell proliferation. J Biol Chem 290:11349-11364.

You L, Yan K, Zou J, Zhao H, Bertos NR, Park M, Wang E, Yang XJ (2015c) The lysine acetyltransferase activator Brpf1 governs dentate gyrus development through neural stem cells and progenitors. PLoS Genet 11:e1005034.

You L, Li L, Zou J, Yan K, Belle J, Nijnik A, Wang E, Yang XJ (2016) BRPF1 is essential for development of fetal hematopoietic stem cells. J Clin Invest 126:3247-3262.

Zagoraiou L, Akay T, Martin JF, Brownstone RM, Jessell TM, Miles GB (2009) A cluster of cholinergic premotor interneurons modulates mouse locomotor activity. Neuron 64:645-662.

Zelikowsky M, Hersman S, Chawla MK, Barnes CA, Fanselow MS (2014) Neuronal ensembles in amygdala, hippocampus, and prefrontal cortex track differential components of contextual fear. J Neurosci 34:8462-8466.

Zhang H, Ben Zablah Y, Zhang H, Jia Z (2021) Rho signaling in synaptic plasticity, memory, and brain disorders. Front Cell Dev Biol 9:729076.

Zhao L, Yang X, Cui L, Wei J, Ni P, Li M, Wang Y, He Y, Li X, Liang S, Tian Y, Wang Q, Cui W, Lin D, Ma X, Li T (2019) Increased expression of a novel miRNA in peripheral blood is negatively correlated with hippocampal volume in patients with major depressive disorder. J Affect Disord 245:205-212.

Zu G, Liu Y, Cao J, Zhao B, Zhang H, You L (2022) BRPF1-KAT6A/KAT6B complex: molecular structure, biological function and human disease. Cancers (Basel) 14:4068.

P-Reviewers: Coppi E, Strogulski NR; C-Editor: Zhao M; S-Editors: Yu J, Li CH; L-Editors: Yu J, Song LP; T-Editor: Jia Y

Additional Table 1 Primer sequence information of RT-qPCR

Target gene	Primer sequence (5'-3')	
	Forward	**Reverse**
Gapdh	AGGTCGGTGTGAACGGATTTG	TGTAGACCATGTAGTTGAGGTCA
Brpf1	TCTGCACAGTCTGAGAGATGAGA	ATCTGACTATGGAGTTCAAGCCC
Wnt6	GCAAGACTGGGGGTTCGAG	CCTGACAACCACACTGTAGGAG
Pitx2	GCAGCCGTTGAATGTCTCTTC	GTCCGTGAACTCGACCTTTTT
Barx1	CGGAGTCGCACCGTATTCAC	TCTTCACCTGTAACTGGCTC
Vax2	GGAGCGGAAGATTTGCGTG	CCTTAGCATCTCGTACCAGGA
Tlx1	CAGCTTCGGTATCGACCAGAT	CTCCAACCAAACAGCCAAGG
Pax2	AAGCCCGGAGTGATTGGTG	CAGGCGAACATAGTCGGGTT
Pax1	CCGCCTACGAATCGTGGAG	CCCGCAGTTGCCTACTGATG
Foxd1	CTTCTCCATCGAGAGCCTCAT	CTGTCCCTTGGTGCAGAGTC
Twist1	GGACAAGCTGAGCAAGATTCA	CGGAGAAGGCGTAGCTGAG
Tbx5	ATGGCCGATACAGATGAGGG	TTCGTGGAACTTCAGCCACAG
Pou4f2	TGGACATCGTCTCCCAGAGTA	GTGTTCATGGTGTGGTAAGTGG
Pcdhga9	CGGGCAAATCCGCTATTCC	ACTTCCACCCCATAAAGTTTCAC
Pcdhgb8	AGCAGCGTGAAGCTAGGGA	GAGTACCGGACTTGCTCTGAG
Wt1	GAGAGCCAGCCTACCATCC	GGGTCCTCGTGTTTGAAGGAA
Klf1	AGACTGTCTTACCCTCCATCAG	GGTCCTCCGATTTCAGACTCAC
Nkx6-3	CGGTGCAGAACTCTTTCTACAA	TGGGAGCTGAGTCCACCAAA
Hoxc8	CTTCGTCAACCCCCTGTTTTC	GTCTTGGACGTGGTGCGAG
Hoxc4	CTACCCTGAGCGTCAGTATAGC	CGCAGAGCGACTGTGATTTCT
Hoxc6	AATTCCACCGCCTATGATCCA	ACATTCTCCTGTGGCGAATAAAA
Hoxc7	TATGTGAACGCGCTTTTTAGCA	GGGGGCTGTTGACATTGTATAA
Hoxc13	GGGGTCGGAATCTAGTCTCCC	CCTCCAAAGTAGCCATAAGGCA
Hoxc9	ACTCGCTCATCTCTCACGACA	AGGACGGAAAATCGCTACAGT
Gja5	GGTCCACAAGCACTCCACAG	CTGAATGGTATCGCACCGGAA
Slc34a2	CCTTGGCCCGAGTTGGAAAAT	CTACAGGAGTCCCGTTGTCAT
Syce3	CTGATTCCGATCCTGGGGAAA	GGTTGCCTGCACTGAGATTTT
Slc45a2	CCGACTGACACCCATACCTAT	ATGCTGTGCATGACAAGTCTC
Synpo21	GGAGGTGCAGGTCACATTAGC	CAAGAAACCCCGTTGATCGC
Uncx	ACCCGCACCAACTTTACCG	TGAACTCGGGACTCGACCA
Chat	CCATTGTGAAGCGGTTTGGG	GCCAGGCGGTTGTTTAGATACA
Illb	GCAACTGTTCCTGAACTCAACT	ATCTTTTGGGGTCCGTCAACT
Adh1	GCAAAGCTGCGGTGCTATG	TCACACAAGTCACCCCTTCTC
Il6	TAGTCCTTCCTACCCCAATTTCC	TTGGTCCTTAGCCACTCCTTC
Pcdhgb4	CCAATGAGTCAACCTCCCATC	TTGCAGCATCTCTGTATCAAACT
Pcdhgb1	AGCCAAGGTCTCTCTAGTGGG	ACGCTGAAATAATCCTCTGCAC
Slco1b2	GGGAACATGCTTCGTGGGATA	GGAGTTATGCGGACACTTCTC
Slco1b5	CATGCTTCTCATCCTGACAAGT	GAGGACGACCTCTGAAGTGG
Slc22a30	GTGGATGTCAGAGTCGGCTC	CCGCTTTCGTAAGATGGGTGT
Slc17a3	GTAGAGATGAGCCCTACAAGTGA	CCATAGCGCATGGAACATAAACT
Slc13a2	CAGGCACTATGGGCCTATCG	AGGATGATGGAGTAAGCACAGT

Slc16a7	GCTGGGTCGTAGTCTGTGC	ATCCAAGCGATCTGACTGGAG
Slc22a18	CACTGGGCCTAGATTCTGTCT	CGCCAGGAAGGAGAGTGAGA
Slc5a8	CGGGACATCGGCAGTTTTG	CTGCGACCGCCCATAAGAA
Fat2	CTTGGCGCTTCACTCACTC	GCTCTGCCAGATACATGCCC
S100a8	AAATCACCATGCCCTCTACAAG	CCCACTTTTATCACCATCGCAA
Rho	CCCTTCTCCAACGTCACAGG	TGAGGAAGTTGATGGGGAAGC
Tight	CCACAGCAGGCACGATAGATA	CATGCCACCCCAGGTCAAC
Lmx1a	ACGGCCTGAAGATGGAGGA	CAGAAACCTGTCCGAGATGAC
Vdr	ACCCTGGTGACTTTGACCG	GGCAATCTCCATTGAAGGGG
Aqp1	AGGCTTCAATTACCCACTGGA	GTGAGCACCGCTGATGTGA
Stx11	TGTCCAGGAGCTATGACCAG	GTTGGTGTCGCGCTTAATGC
Zic1	CAGTATCCCGCGATTGGTGT	GCGAACTGGGGTTGAGCTT
Robo3	AGATGAACTTGTTCGCGGACT	GGAAGCAGACTAGGGTTGAGC
Cdb16	CTCCAGCCTCTCAACGATTCC	GGTGCGTGAACACAAGAATGA
Pcp2	ATGGACGACCAGCGTGTAAC	CCTTGGGGCCGATAGGTTG

Additional Table 3 GO-BP of upregulated and downregulated DEGs of 2-month-old cKO vs. WT hippocampal CA1 tissue by mRNA sequencing

Category	Term	Count	%	PValue	Genes	List Total	Pop Hits	Pop Total	Fold Enrichment	Bonferroni	Benjamini	FDR
Upregulated GO-BP												
GOTERM_BP_DIRECT	GO:0045893~positive regulation of transcription, DNA-templated	6	0.041445	0.00574	WNT6, MYOCD, WT1, WBP2NL, PITX2, KLF1	34	712	20094	4.980337	0.89527	0.612679	0.612679
GOTERM_BP_DIRECT	GO:0016055~Wnt signaling pathway	4	0.02763	0.006809	WNT6, PITX2, BARX1, VAX2	34	237	20094	9.974684	0.93132	0.612679	0.612679
GOTERM_BP_DIRECT	GO:0001570~vasculogenesis	3	0.020723	0.006909	MYOCD, WT1, PITX2	34	76	20094	23.32895	0.933984	0.612679	0.612679
GOTERM_BP_DIRECT	GO:0043010~camera-type eye development	3	0.020723	0.00763	WT1, PITX2, VAX2	34	80	20094	22.1625	0.950326	0.612679	0.612679
GOTERM_BP_DIRECT	GO:0007267~cell-cell signaling	3	0.020723	0.007815	WNT6, GJA5, BARX1	34	81	20094	21.88889	0.95383	0.612679	0.612679
GOTERM_BP_DIRECT	GO:0032815~negative regulation of natural killer cell activation	2	0.013815	0.011441	CLNK, LILRB4A	34	7	20094	168.8571	0.98901	0.619275	0.619275
GOTERM_BP_DIRECT	GO:0045944~positive regulation of transcription from RNA polymerase II promoter	7	0.048353	0.013147	MYOCD, IFI207, CREB3L3, WT1, PITX2, HOXA7, KLF1	34	1216	20094	3.402138	0.994416	0.619275	0.619275
GOTERM_BP_DIRECT	GO:0006357~regulation of transcription from RNA polymerase II promoter	8	0.05526	0.01388	MYOCD, CREB3L3, WT1, PITX2, BARX1, HOXA7, VAX2, KLF1	34	1606	20094	2.94396	0.995828	0.619275	0.619275
GOTERM_BP_DIRECT	GO:0006355~regulation of transcription, DNA-templated	7	0.048353	0.014218	CREB3L3, WT1, PITX2, BARX1, HOXA7, VAX2, KLF1	34	1237	20094	3.344382	0.996352	0.619275	0.619275
GOTERM_BP_DIRECT	GO:0055123~digestive system development	2	0.013815	0.016306	PITX2, BARX1	34	10	20094	118.2	0.998411	0.638672	0.638672
GOTERM_BP_DIRECT	GO:0035886~vascular smooth muscle cell differentiation	2	0.013815	0.017922	MYOCD, PITX2	34	11	20094	107.4545	0.999166	0.638672	0.638672
GOTERM_BP_DIRECT	GO:0000122~negative regulation of transcription from RNA polymerase II promoter	6	0.041445	0.020416	MYOCD, IFI207, WT1, PITX2, HOXA7, VAX2	34	975	20094	3.636923	0.999692	0.666932	0.666932
GOTERM_BP_DIRECT	GO:0007601~visual perception	3	0.020723	0.02575	CRYGA, GJA5, VAX2	34	152	20094	11.66447	0.999964	0.776448	0.776448
GOTERM_BP_DIRECT	GO:0098869~cellular oxidant detoxification	2	0.013815	0.032353	NNT, PRDX6B	34	20	20094	59.1	0.999997	0.905891	0.905891

Downregulated GO-BP													
GOTERM_BP_DIRECT	GO:0045429~positive regulation of nitric oxide biosynthetic process	4	0.014427	7.28E-04	IL6, ITGB2L, AGXT2, IL1B	69	52	20094	22.40134	0.34051	0.416138	0.416138
GOTERM_BP_DIRECT	GO:0019626~short-chain fatty acid catabolic process	2	0.007213	0.006757	CES1D, CES1F	69	2	20094	291.2174	0.979309	1	1
GOTERM_BP_DIRECT	GO:0071549~cellular response to dexamethasone stimulus	3	0.01082	0.010171	IL6, METTL21C, AQP1	69	45	20094	19.41449	0.997114	1	1
GOTERM_BP_DIRECT	GO:0045766~positive regulation of angiogenesis	4	0.014427	0.017305	ITGB2L, IL1B, CAMP, AQP1	69	161	20094	7.235215	0.999954	1	1
GOTERM_BP_DIRECT	GO:0032757~positive regulation of interleukin-8 production	3	0.01082	0.018161	IL6, IL1B, CAMP	69	61	20094	14.32217	0.999972	1	1
GOTERM_BP_DIRECT	GO:0015793~glycerol transport	2	0.007213	0.020136	AQP7, AQP1	69	6	20094	97.07246	0.999991	1	1
GOTERM_BP_DIRECT	GO:0090205~positive regulation of cholesterol metabolic process	2	0.007213	0.023453	CES1D, CES1F	69	7	20094	83.20497	0.999999	1	1
GOTERM_BP_DIRECT	GO:0010573~vascular endothelial growth factor production	2	0.007213	0.023453	IL6, IL1B	69	7	20094	83.20497	0.999999	1	1
GOTERM_BP_DIRECT	GO:0030198~extracellular matrix organization	4	0.014427	0.024515	COL4A4, COL4A3, GM21983, COL6A5	69	184	20094	6.330813	0.999999	1	1
GOTERM_BP_DIRECT	GO:0032496~response to lipopolysaccharide	4	0.014427	0.025559	IL1B, SLCO1B2, BDKRB1, S100A8	69	187	20094	6.229249	1	1	1
GOTERM_BP_DIRECT	GO:0070295~renal water absorption	2	0.007213	0.026759	AQP7, AQP1	69	8	20094	72.80435	1	1	1
GOTERM_BP_DIRECT	GO:0042102~positive regulation of T cell proliferation	3	0.01082	0.027383	IL6, CD59B, IL1B	69	76	20094	11.49542	1	1	1
GOTERM_BP_DIRECT	GO:0030593~neutrophil chemotaxis	3	0.01082	0.030797	ITGB2L, IL1B, S100A8	69	81	20094	10.78583	1	1	1
GOTERM_BP_DIRECT	GO:0050691~regulation of defense response to virus by host	2	0.007213	0.033338	IL1B, IFNLR1	69	10	20094	58.24348	1	1	1
GOTERM_BP_DIRECT	GO:0070857~regulation of bile acid biosynthetic process	2	0.007213	0.033338	CES1D, CES1F	69	10	20094	58.24348	1	1	1

GOTERM_BP_DIRECT	GO:0032836~glomerular basement membrane development	2	0.007213	0.033338	COL4A4, COL4A3	69	10	20094	58.24348	1	1	1
GOTERM_BP_DIRECT	GO:0051791~medium-chain fatty acid metabolic process	2	0.007213	0.03661	CES1D, CES1F	69	11	20094	52.94862	1	1	1
GOTERM_BP_DIRECT	GO:0097398~cellular response to interleukin-17	2	0.007213	0.039872	IL6, IL1B	69	12	20094	48.53623	1	1	1
GOTERM_BP_DIRECT	GO:0006954~inflammatory response	5	0.018034	0.043122	IL6, ITGB2L, IL1B, BDKRB1, S100A8	69	390	20094	3.733556	1	1	1
GOTERM_BP_DIRECT	GO:0010923~negative regulation of phosphatase activity	2	0.007213	0.043124	SH3RF2, SH2D4A	69	13	20094	44.80268	1	1	1
GOTERM_BP_DIRECT	GO:0042448~progesterone metabolic process	2	0.007213	0.046364	HSD3B4, AKR1C14	69	14	20094	41.60248	1	1	1
GOTERM_BP_DIRECT	GO:0010887~negative regulation of cholesterol storage	2	0.007213	0.049593	CES1D, CES1F	69	15	20094	38.82899	1	1	1

Additional Table 4 The selected DEGs from RNA-Seq validated by RT-qPCR

Gene	RNA-Seq (fold)	RT-qPCR (fold)
Brpf1	0.7	0.4±0.1***
Wnt6	3.9	1.1±0.5
Pitx2	8.7	643.3±501.6
Vax2	5.9	334.7±186.7
Tlx1	21	10.0±6.3
Pax2	19.3	646.3±501.6
Pax1	12	3.8±1.3*
Foxd1	3.8	3.6±4.7
Twist1	3.5	3.0±1.2*
Tbx5	10.6	0.6±0.3
Pou4f2	10.3	11.3±7.1
Pcdhga9	9.6	0.7±0.1**
Pcdhgb8	5.7	0.6±0.2
Wt1	6.3	0.7±0.8
Klf1	6.1	0.8±0.4
Nkx6-3	4.5	1.0±0.5
Hoxc8	3.3	1.1±0.2
Hoxc4	19.7	1.5±1.0
Hoxc6	12	58.2±42.2
Hoxa7	7	5.9±5.0
Hoxb13	5.3	107.2±93.8
Hoxc9	3.9	2.5±2.3
Gja5	5.1	0.8±0.2
Slc34a2	3.7	0.6±0.5
Syce3	3.1	0.9±0.2
Slc45a2	3.1	1.3±0.9
Synpo21	2.8	2.5±2.3
Uncx	0.2	0.4±0.4
Chat	0.2	1.3±1.7
Il1b	0.3	0.6±0.2**
Adh1	0.3	0.7±0.5
Il6	0.3	0.8±0.1***
Pcdhgb4	0.3	1.0±0.1
Pcdhgb1	0.1	0.6±0.1***
Slco1b2	0.3	0.7±0.5
Slco1a5	0.3	1.4±1.3
Slc22a30	0.3	0.6±0.7
Slc16a7	0.4	0.7±0.1**
Slc22a18	0.4	0.8±0.5
Rho	0.3	0.5±0.2*
Tigit	0.3	0.5±0.1**
Lmx1a	0.4	1.0±0.6
Vdr	0.4	0.5±0.4
Stx11	0.4	0.5±0.4

Zic1	0.4	0.5±0.4
Robo3	0.5	0.3±0.1***
Pcp2	0.5	0.6±0.3

For RT-qPCR, data are expressed as mean ± SD (n =3 pairs).*P < 0.05, **P < 0.01, ***P < 0.001 (Student's t-test).

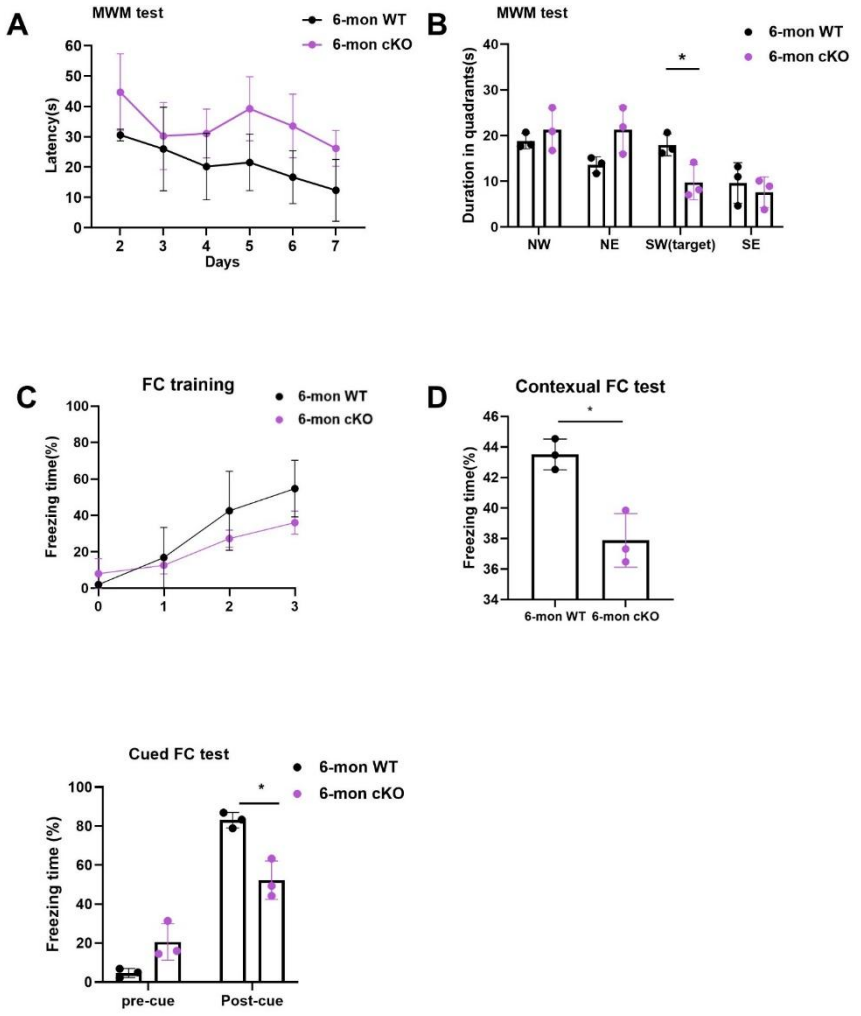

Additional Figure 1 Morris water maze and fear conditioning test results in 6-month-old WT and cKO mice.

(A) Statistical comparison of the latency to reach the hidden platform in the MWM tests (n = 3 mice for each group). (B) Statistical comparison of the duration spent in each of the 4 quadrants in the MWM tests (*n* = 3 mice for each group). (C) Statistical comparison of the percentage of freezing time during the phase of fear memory acquisition in contextual and cued fear conditioning tests (n = 3 mice for each group). (D) Statistical comparison of the percentage of freezing time in a scene fear memory (contextual) test (*n* = 3 mice for each group). (E) Statistical comparison of the percentage of freezing time in a sound fear memory (cued) test (*n* = 3 mice for each group). Data are expressed as mean ± SD. **P* < 0.05 (two-way analysis of variance with Bonferroni post hoc test). *Brpf1:* Bromodomain and PHD finger containing protein 1; FC: fear conditioning; MWM: Morris water maze; NE: northeast; NW: northwest; SE: southeast; SW (target): southwest; WT: wild type.